Soils and Rocks
An International Journal of Geotechnical and Geoenvironmental Engineering
www.soilsandrocks.com
ISSN 1980-9743
ISSN-e 2675-5475

Micro to macro investigation of clays advising their constitutive modelling - part I

Federica Cotecchia[1], Simona Guglielmi[2#], Francesco Cafaro[1], Antonio Gens[3]

Article

Keywords
Microstructure
Constitutive modeling
Soil microstructure analysis

Abstract

This keynote lecture discusses the results of a long lasting experimental research, devoted to the investigation of clay microstructure and its evolution upon loading. Micro-scale analyses, involving scanning electron microscopy, image processing, mercury intrusion porosimetry and swelling paths to test the clay bonding, are presented on clays subjected to different loading paths, with the purpose of providing experimental evidence of the processes at the micro-scale which underlie the clay response at the macro-scale. Data from the literature on clays of different classes, either soft or stiff, are compared to original results on two stiff clays, Pappadai and Lucera clay, both in their natural state and after reconstitution in the laboratory. The results presented herein allow building a conceptual model of the evolution of clay microstructure upon different loading paths, providing microstructural insights into the macro-behaviour described by constitutive laws and advising their mathematical formalization in the framework of either continuum mechanics or micro-mechanics. For editorial purposes, the research results are presented in two parts. The first part, presented in this paper, concerns the results for reconstituted clays, whereas a second part, concerning the corresponding natural clays, is discussed in a second companion paper.

1. Introduction: background and research perspectives

This keynote lecture reports on research concerned with the correspondence between the engineering behaviour of clays, at the scale of the representative element volume (REV – macro-behaviour), and the multi-scale and multi-physics processes controlling such behaviour. The main objective is to provide experimental evidence of the micro-scale processes which determine the response of consolidated clays, to support the mathematical formalization of their constitutive laws, either in the framework of continuum mechanics, or in that of micro-mechanics (Figure 1).

For natural clays, far more than for clean coarse soils, the engineering response depends not only on the grain, or particle, size distribution and mineralogy, but also on physical and chemical processes taking place in the clay history since deposition, which impact its microstructure. This has been defined (e.g., Lambe & Whitman, 1969) as a combination of fabric (i.e., the geometric arrangement of the soil particles and grains) and bonding (i.e., the inter-particle forces), where clay bonding is not necessarily of a mechanical nature (Cotecchia & Chandler, 2000). Hence, in this research, the interpretation of the micro-scale processes determining the clay macro-behaviour has been always based upon, on one side, the direct investigation of the microstructural features, according to the scientific literature in clay micro-morphology and clay physics and, on the other, the knowledge of the clay history since deposition, i.e., the geological history for natural clays. The results of such interpretations can then be used to characterize the correspondence between classes of clays, of given composition, background history and achieved microstructural features, and classes of macro-behaviour.

Relating classes of macro-behaviour to classes of clays may support the use, in the engineering practice, of existing constitutive laws developed in the framework of continuum mechanics and elasto-plasticity (Figure 1, research line a-*i*). This is the case if, for constitutive laws (e.g., Schofield & Wroth, 1968; Roscoe & Burland, 1968; Gens & Potts, 1988; Gens & Nova, 1993; Rouainia & Wood, 2000; Kavvadas & Amorosi, 2000; Baudet & Stallebrass, 2004) resulting from macro-behaviour studies (to date calibrated only based on macro-scale data and optimization strategies, e.g., Borja et al., 1997; Zhang et al., 2009; Knabe et al., 2013), the set of parameter values required to predict the class of macro-behaviour relating to clay class is provided.

#Corresponding author. E-mail address: simona.guglielmi@poliba.it
[1]Politecnico di Bari, Dipartimento di Ingegneria Civile, Ambientale, del Territorio, Edile e di Chimica, Bari, Italy.
[2]Direzione Generale per le Dighe e le Infrastrutture Idriche, Ministero delle Infrastrutture e dei Trasporti, Roma, Italy.
[3]Universitat Politécnica de Catalunya, Departamento de Ingeniería Civil y Ambiental, Barcellona, Spain.

Submitted on December 5, 2023; Final Acceptance on January 30, 2024; Discussion open until November 30, 2024.

https://doi.org/10.28927/SR.2024.011723

Also, the knowledge of the physical background of a given class of macro-response could support further development of the constitutive laws, e.g., implementing additional microstructure constitutive variables in the hardening law (Figure 1, research line a-*ii*). On the other hand, the identified relations between classes of clays, macro-response and micro-scale processes, may support the integration of micro-mechanics in the constitutive modelling of clays (Figure 1, research line b).

Background of the presented research work is the geotechnical studies of the effects of composition, deposition and consolidation conditions on the clay response (e.g. Skempton & Northey, 1952; Bjerrum, 1967; Schmertmann, 1969; Pusch, 1970; Skempton, 1970), which, since the early fifties, have shown the differences in macro-response of natural and reconstituted clays. The research insight into these differences (Burland, 1990; Leroueil & Vaughan, 1990; Hight et al., 1992; Smith et al., 1992; Cotecchia & Chandler, 1997, 2000; Cafaro & Cotecchia, 2001; Gasparre et al., 2007) has given evidence to the important influence on clay macro-response of non-mechanical processes taking place in the geological history of natural clays (e.g., thixotropy, diagenesis, weathering). Accordingly, the comparison between the macro-behaviour of natural and reconstituted clays has proved a useful method to investigate the mechanical effects of differences in microstructure, once these are characterized through micro-scale studies of the natural clay and of the same clay when reconstituted.

Background of the presented research work is also the direct investigations of clay microstructure developed since the availability of scanning electron microscopy, SEM. In the late seventies, pioneer SEM applications to the investigation of the effects of loading on clay microstructure, i.e., post-mortem investigations (Tovey, 1973; Sfondrini, 1975; Tavenas et al., 1979; Sides & Barden, 1971; Mitchell, 1976; Smart & Tovey, 1981; Cotecchia et al., 1982; Delage & Lefebvre, 1984), already provided evidence of the microstructural changes in the background of given clay stress-strain responses. Since then, SEM, later combined with Mercury Intrusion Porosimetry, MIP (Diamond, 1970; Romero & Simms, 2008), have been used in experimental studies of the dependence of clay macro-behaviour on clay microstructure (e.g., Delage & Lefebvre, 1984; Griffiths & Joshi, 1990; Locat, 1995; Lapierre et al., 1990; Cotecchia & Chandler, 1997, 1998; Delage, 2010; Hattab & Fleureau, 2010; Hicher et al., 2000; Cetin, 2004; Monroy et al., 2010; Hattab et al., 2013; Cotecchia et al., 2016, 2019; Mitaritonna et al., 2014; Guglielmi et al., 2018, 2023, 2024; Jia et al., 2020).

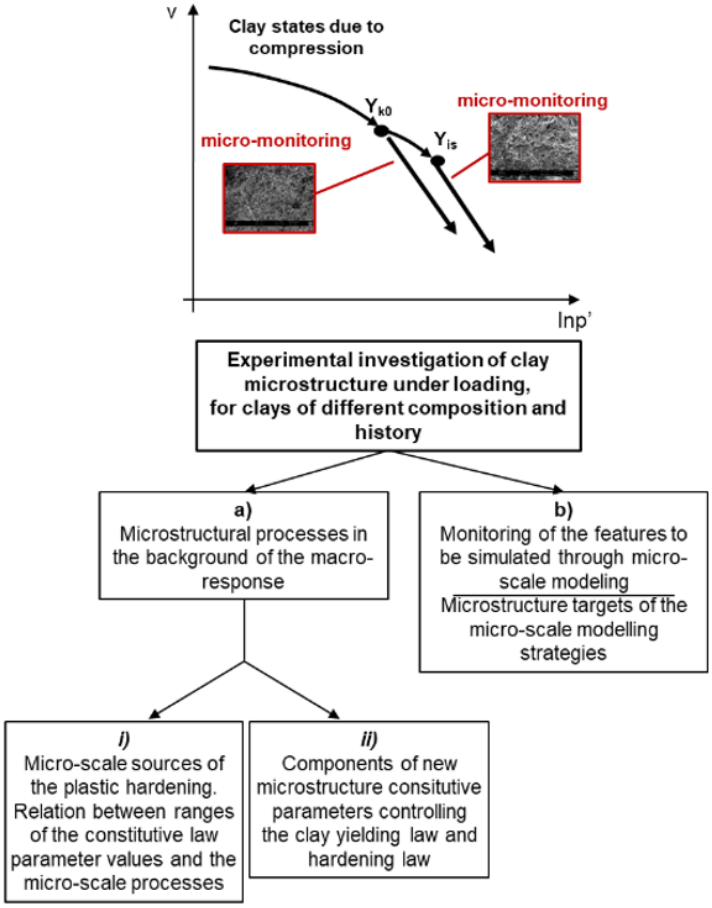

Figure 1. Research lines (a) and (b) of reference in the lecture.

Nonetheless, the exploration of micro-mechanical modelling of clays has become a main research issue only in the last decade, prompted by the parallel intense development of micro-mechanical modeling of coarse soil behaviour. The latter has indeed resulted from long-lasting research (e.g., Oda, 1972, 1993; Cundall & Strack, 1979; Oda et al., 1985; Wan et al., 2005; La Ragione & Jenkins, 2007; Li & Li, 2009), boosted recently thanks to new techniques revealing grain-scale processes in these geomaterials (Desrues et al., 2010; Hall et al., 2010; Andò et al., 2013; Viggiani et al., 2015; Guida et al., 2018; Nardelli & Coop, 2019).

It must be acknowledged, though, that the electro-chemo-mechanical processes taking place at colloidal scale in clays, subject of sciences such as clay mineralogy, crystallography, colloid behaviour and micro-morphology (e.g., Gouy, 1910; Chapman, 1913; Derjaguin & Landau, 1941; Verwey & Overbeek, 1948; Sides & Barden, 1971; Collins & McGown, 1974; Gay & Berne, 1981; O'Brien & Slatt, 1990; Gupta et al., 2011; Israelachvili, 2011), make the simulation of clay macro-behaviour through the modelling of micro-scale processes a challenge, much more complex than for coarse soils. Such modelling needs to be strongly interdisciplinary and involve systemic experimental investigation of the micro-scale processes for different classes of clays. In any case, the micro to macro investigation of clays, making use of SEM and MIP to assess the effects of loading on clay microstructure, are still too few to date.

The limited number of post-mortem micro-analyses of clays is due to the great effort required by such studies. These require the cryo-liofilization of small clay specimens to be performed according to an appropriate protocol (Gillott, 1970; Delage & Pellerin, 1984; Delage & Lefebvre, 1984; Penumadu & Dean, 2000; Cuisinier & Laloui, 2004; Mitchell & Soga, 2005; Sasanian & Newson, 2013; Romero & Simms, 2008; Guglielmi et al., 2024) not to disturb the clay microstructure; doubts about its effects on clay slurry remain (Deirieh et al., 2018). Furthermore, relating micro-processes to clay macro-behaviour through post-mortem micro-analyses requires a great number of tests, since tests must stop at different stages of loading. In addition, a successful SEM application requires collaboration between geotechnical researchers, microscopy analysts and mineralogists. Given so, the use of alternative less-invasive technologically advanced techniques to achieve continuous knowledge of the clay fabric changes all the way through loading paths, such as X-ray Computed Tomography, Small Angle X-ray scattering (Birmpilis et al., 2019, 2022a, b) has been attempted in micro-macro investigation of clays. However, to date, 'in-operando' techniques attain very coarse spatial resolution in clays, which makes them not satisfactory for clay fabric analyses.

The mathematical modelling of clay micro-scale processes has been so far attempted through the use of the Derjaguin-Landau-Vervey-Overbeek, DLVO, model to predict non-contact forces between clay particles. Due to the limitations of the employed theoretical assumptions, such attempts have addressed mono-mineral clay particles within simple, strictly defined scenarios (e.g., Anandarajah, 1994, 2000; Yao & Anandarajah, 2003; Frenkel & Smit, 2013 Ebrahimi et al., 2012, 2014, 2016; Liu et al., 2015; Sjoblom, 2016). Other modelling strategies entail the application of the distinct element method, DEM, to clay micro-mechanics, simplifying the inter-particle forces through equivalent mechanical elements, to be calibrated based upon either phenomenological assumptions or empirical observations (Pedrotti & Tarantino, 2018; Pagano et al., 2020). Although Molecular Dynamics, MD (Alder & Wainwright, 1959; Frenkel & Smit, 2013), is generally used for intra-particle phenomena, recent studies have explored the implementation of the DLVO theory to calibrate potential functions within molecular dynamics deployed between particles (simulated as platelets), even endorsing the implementation of the Gay-Berne potential (Ebrahimi et al., 2014; Bandera et al., 2019, 2021). Whichever micro-scale modelling strategy, though, still requires a deeper experimental insight into the clay fabric and bonding evolutions under loading to be taken as the target of the model predictions (Figure 1, research line b). To date, for multi-mineral clays, either reconstituted or natural, such insight may be still pursued solely through post-mortem micro-analyses.

In order to progress in this direction, the research work here of reference has entailed post-mortem micro-analyses of clay specimens of varying composition, either reconstituted in the laboratory or natural, both at early stages of consolidation and after compression under different constant stress ratios, η. For editorial purposes, the research results have been split in two parts. The first part, presented in this paper, concerns the results for reconstituted clays, whereas the second part, concerning the corresponding natural clays is discussed in a second companion paper. The research methodology, adopted for both the studies, on the natural and the reconstituted clays, is presented in the following section of this paper.

The investigation results provide evidence of how the interaction forces between the clay components determine different clay states (in the compression plane) and fabrics for varying composition, deposition environment (laboratory or field), constant stress ratio (η) compression and other processes taking place at the micro-scale under burial. The micro-scale investigations have made use of SEM and field emission SEM (FESEM; Gillott, 1973; Tovey & Wong, 1973), MIP (Diamond, 1970) and swelling tests (to assess the clay bonding strength; Burland, 1990). To quantify the fabric orientation, SEM and FESEM micrographs have been subjected to image processing (e.g., Martinez-Nistal et al., 1999; Hattab & Fleureau, 2010).

The micro-analysis results are intended to support advances for both research lines in Figure 1. For line a-*i*, they can support the use, in engineering design (e.g., Manzano et al., 2023), of constitutive laws in the framework of elasto-plasticity, since the knowledge of the micro-processes generating a prediction

achieved through a given set of parameter values, provides the engineer with a guidance to the selection of the appropriate parameter values. Furthermore, according to line a-*ii*, the results provide indications about microstructure constitutive parameters (either scalar or tensorial) useful to represent clay microstructure in new hardening laws (e.g., for sands: Oda et al., 1980; Oda, 1993). For clay micro-scale modelling (Figure 1, line b), the research results outline the main micro-scale processes impacting the clay macro-response, which could guide the design of such modeling.

2. Research methodology

The experimental data discussed in both companion papers (for either reconstituted or natural clays) resulted either from tests performed by the authors, or from previous published studies of other authors. In any case, the clay composition is always characterized through mineralogical and chemical analyses and geotechnical index tests (liquid and plastic limits, w_L and w_P, grading fractions, e.g., clay fraction *CF*). The clay macro-state is always characterized in terms of void ratio, *e*, and degree of saturation, S_r. Furthermore, the clay history is characterized providing: i) the original deposition conditions, ii) the preconsolidation pressure, iii) subsequent unloading/loading sequences, iv) ageing and diagenesis for the natural clays. The clay class of the specific clay under study is then identified, accordingly.

For each clay of reference, a set of one-dimensional compression tests has been carried out, together with micro-analyses to assess the clay fabric and bonding at different stages of compression. For some of the clays, one-dimensional swelling has also been performed to characterize the clay bonding strength through the swell sensitivity C_s^*/C_s (Schmertmann, 1969), since the strengthening of bonding which may develop in the natural clay tends to restrain the swell capacity. Also, different η compressions have been performed to investigate the influence of η on the clay microstructure (degree of fabric orientation and degree of mechanical anisotropy).

For most clay prototypes, the macro-tests and the micro-analyses have been carried out on both the natural and the reconstituted clay, since the comparison between the macro-behaviour and the microstructural features of the natural and the reconstituted clay provide evidence of the micro-structure effects on the clay macro-response. The reconstituted clay data are discussed in the following, while those for the natural clays are compared with the following in the companion paper. In both papers the constitutive modelling implications of the micro-scale findings are explored.

2.1 Micro-scale investigation techniques

Different techniques have been combined to investigate the clay microstructure post-mortem. The specimens have been unloaded in undrained conditions at the end of the test and cube-shaped specimens of ≈1 cm^3 volume have been cut from their central part. Before microstructural testing, the small specimens were subjected to freeze-drying. This is routinely used for sample dehydration, to minimize the clay disturbance compared to air, or oven drying (Gillott, 1970; Delage & Pellerin, 1984; Delage & Lefebvre, 1984; Penumadu & Dean, 2000; Cuisinier & Laloui, 2004; Mitchell & Soga, 2005; Sasanian & Newson, 2013; Romero & Simms, 2008).

MIP data provide the clay pore size density function, PSD. SEM (after specimen gold coating), or FESEM (carbon coating) micrographs have been acquired for vertical fractures of the freeze-dried specimens, obtained by fracturing the soil before coating.

Fabric orientation, which may represent an internal source of anisotropy of both mechanical and hydraulic properties, has been assessed not only qualitatively (e.g., Delage & Lefebvre, 1984; Lima et al., 2008; Cotecchia et al., 2016), but also quantitatively, using image processing. This has been performed through a digital operator-independent technique (Martinez-Nistal et al., 1999; Mitaritonna et al., 2014; Cotecchia et al., 2019), successfully applied to clays in the past (e.g., Pisa clay and Pappadai clay; Veniale et al., 1993, 1995; Cotecchia & Chandler 1997, 1998) and extensively illustrated by Mitaritonna et al. (2014) and Cotecchia et al. (2019). The procedure is based on the thinning of the elongated bright regions of the micrograph, which represent the edges of oriented particle aggregates, as exemplified by Cotecchia et al. (2019)[1] and Guglielmi et al. (2024)[2]. The resulting field of vectors is processed to derive a histogram of orientations (rosette) and a scalar statistical expression of the dispersion of the vectors with respect to the mean direction, *L*. *L* has a value of 1 for a completely iso-oriented fabric and it decreases for 'low oriented' ($0.15 < L < 0.21$) and 'randomly oriented' ($L < 0.15$) fabric (Martinez-Nistal et al., 1999).

3. The micro-scale REV

Cotecchia et al. (2019) discuss post-mortem microstructural analyses of Pappadai clay, in its natural and reconstituted state, with the aim of characterizing the micro-scale sources of the clay macro-behaviour in compression. The authors discuss the clay fabric features, through qualitative and quantitative investigations of the SEM micrographs, and provide elements characterizing the bonding of the clay when natural, through: 1) its inspection in SEM using energy-dispersive X-ray spectroscopy, EDS; 2) the measurement of C_s^*/C_{si}; 3) the comparison of the overconsolidation ratio due to geological loading processes, *OCR* ($= \sigma'_p/\sigma'_{v0}$, where σ'_p is the preconsolidation pressure and σ'_{v0} the *in situ* vertical effective stress), and the yield stress ratio of the clay in compression, $YSR = \sigma'_y/\sigma'_{v0}$. The

[1] See Figure 3 in Cotecchia et al. (2019).
[2] See Figure 2 in Guglielmi et al. (2024).

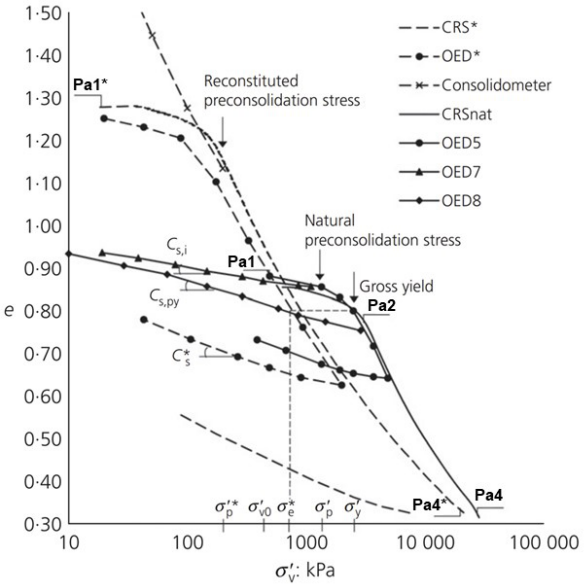

Figure 2. 1D behaviour of Pappadai clay in the [e; σ'_v] plane (modified after Cotecchia et al., 2019).

monitoring of C_s^*/C_{si} under loading provides indications of the bonding evolution with compression. Figure 2 shows the results of 1D compression and swelling tests on natural and reconstituted Pappadai clay and the clay states for which the authors discuss the micro-scale data.

The state of the natural clay (Pa1 in the figure) resulted from its geological overconsolidation (Cotecchia & Chandler, 1995; OCR = 3). When subjected to 1D compression, the clay exhibits gross yield (onset of major decay in stiffness; Hight et al., 1992), at σ'_y about twice σ'_p ($YSR \approx 2 \cdot OCR$), as a result of diagenesis under burial, which has increased the strength of the clay bonding. Through EDS, Cotecchia (1996) shows that the clay bonding increased its strength during diagenesis, partly as an effect of the development of an amorphous calcite film, binding the natural clay particles.

The reconstituted Pappadai clay (parameters*), prepared according to Burland (1990), exhibits a swelling index compatible with $C_s^*/C_{si} = 2.5$, which confirms the existence of an additional bonding in the natural clay, characterized through EDS as said above. It allows the natural fabric to achieve higher void ratio than the reconstituted along compression paths, providing the clay with a stress sensitivity, $S_\sigma = \sigma'_y/\sigma^*_e$ (where σ^*_e is the pressure on the ICL for the same void ratio of the natural clay at gross yield) of 3.5 (Figure 2).

The size of the minimum clay volume including a representative distribution of all the bonding and fabric features recurring in the clay microstructure, clay Micro-REV, has been investigated by Cotecchia et al. (2019) for both the natural and reconstituted Pappadai clay characterized above. To this aim, the authors investigate, in the SEM, the recurrence across the specimens of both the fabric and the bonding features, the latter using EDS.

The reconstituted clay 1D pre-compressed to $\sigma'_v = 200$kPa and then swelled to Pa1* in Figure 2, is found to embody fabric features like those exemplified in Figure 3a, showing a vertical fracture of about 10^4 μm^2 size area (cubic volume 10^{-3} mm^3), investigated at a 'medium scale' of 10^3 magnification (Collins & McGown, 1974; O'Brien & Slatt, 1990). Such fabric exhibits a repetitive pattern, formed of densely packed domains in face to face contact forming stacks (Figures 3b and 3e), confining either macro-pores (diameter above 1 μm; Matsuo & Kamon, 1977; Guglielmi et al., 2018), or aggregates of randomly oriented particles/domains, in edge to face contact. The image processing of several medium scale micrographs of Pa1* delivers repetitive L values, in the narrow range 0.23-0.27 (e.g., Figure 3c), which suggests a repetitive medium-good orientation at this scale (Martinez-Nistal et al., 1999). A repetitive porosimetry is expected to correspond to such a fabric pattern.

For the natural clay at state Pa1 ($e = 0.88 - \sigma'_v = 414$ kPa; Figure 2), both the qualitative analysis and the image processing of several medium scale micrographs result in a repetitive fabric too. This is formed by a dense packing of stacks, locally burying either randomly oriented domains (e.g., bookhouse, Figure 3e), or macropores, or micro-fossils (Cotecchia et al., 2019[3]). The direction histograms deliver repetitive values of L in the range 0.24-0.37, indicative of a good orientation fabric. At higher magnifications (i.e., 10^4-10^5; clay portions of about 10^{-6} mm^3 volume; 'large scale'), in either the reconstituted specimen Pa1*, or the natural Pa1, the fabric is highly variable, from a complete preferred orientation, c.p.o., to a randomly oriented fabric, as exemplified in the figures reported by Cotecchia et al. (2019)[4]. Accordingly, for both clays, the image processing at large scale results in variable indices of orientation, $0.15 < L < 0.28$. Similarly to both Pa1* and Pa1, at high pressure, e.g. samples Pa4* and Pa4 in Figure 2, the medium scale fabric is still not uniform and, at large scale, the image processing detects highly variable L values.

The authors find that such variability in local fabric generally applies to natural and reconstituted clays 1D compressed to medium-high pressures (Guglielmi et al., 2024), providing evidence of the crucial need for a characterization of the micro-scale features within a micro-REV of the clay, if wishing to assess the micro-scale sources of the clay macro-behaviour. The micro-REV structure must include, in a repetitive way, the different local fabric and bonding features, to fulfil the role of internal variable controlling the clay macro-behaviour. For Pappadai clay, either natural or reconstituted, Cotecchia et al. (2019) show that the micro-REV size is larger than 10^{-6} mm^3, corresponding to clay fractures of about 10^{-3} mm^3 size, examined at the medium-scale. Mitaritonna et al. (2014) are the first

[3] See Figure 5 in Cotecchia et al. (2019).
[4] See Figure 6 in Cotecchia et al. (2019).

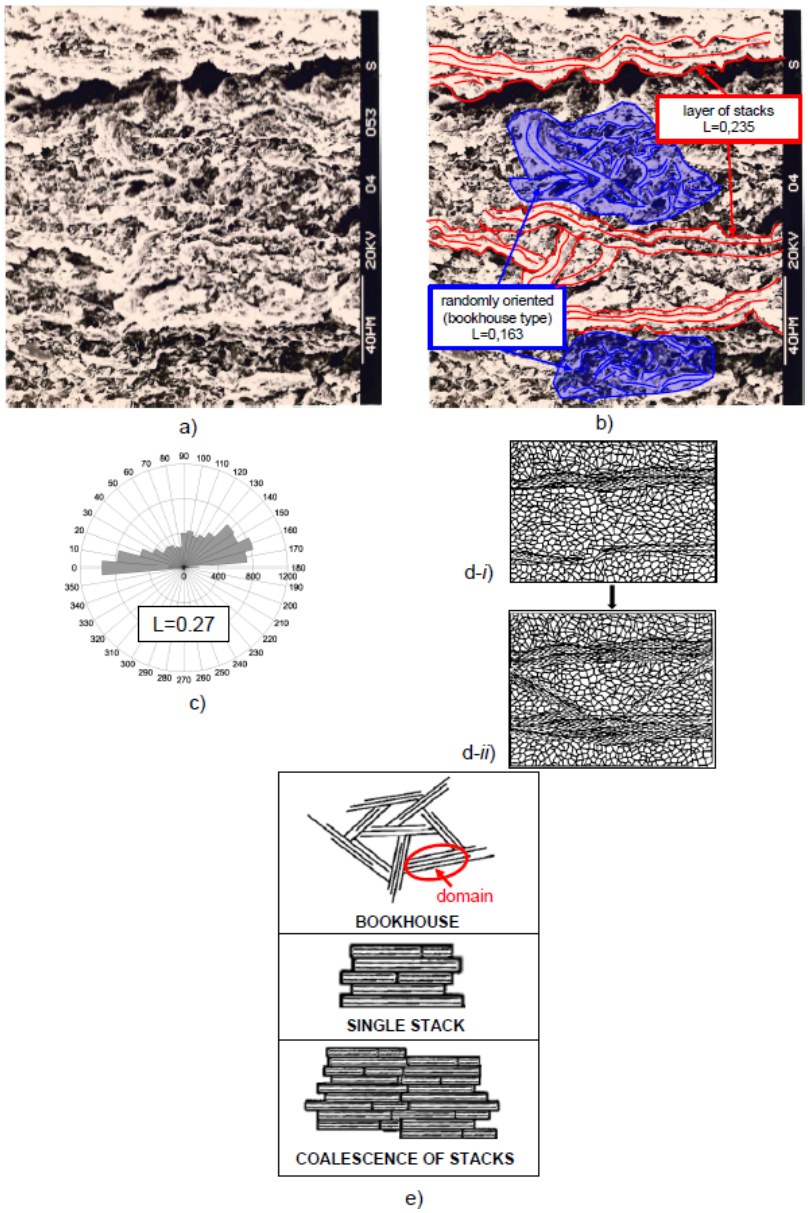

Figure 3. (a) Micro-REV fabric of reconstituted Pappadai clay (Pa1* in Figures 2 and 5), with (b) examples of different local fabric arrangements and local L values; (c) corresponding direction histogram and index of fabric orientation (modified after Cotecchia et al., 2019 and Guglielmi et al., 2024); (d-*i*) 1D compressed clay fabric scheme, after Sfondrini (1975), and (d-*ii*) its evolution in 1D compression; (e) fabric components (sketches from Sides & Barden, 1971, modified).

to provide evidence of how the clay macro-behaviour relates to the medium-scale clay fabric features, i.e., the micro-REV fabric, as further explored in the following sections.

All the results discussed above suggest a possible strategy to define the microstructure constitutive parameters, which may be either scalar or tensorial functions indicative of the influence of fabric and bonding on the clay hardening law, in macro-behaviour constitutive laws (Figure 1, research line a). These functions could formalize the influence of the degree of orientation of the micro-REV fabric, L, for medium magnification SEM micrographs, or the influence of the micro-REV porosimetry, on the macro-response. The microstructure constitutive parameters should embody also the current bonding strength, although the quantitative characterization of bonding through micro-scale observations is not pursued yet through micro-scale investigations. Further research is still necessary for the acquisition of a database of micro-scale observations sufficient for the characterization of the microstructure parameters recalled above. To date, such a database is achievable only through post-mortem testing. The analyses of post-mortem test data

reported in the following are intended to contribute to the reaching of those objectives.

It is worth highlighting that the micro-REV scale is smaller than the scale of the single particle interactions. Hence, after the very early stage of initial deposition, the set of micro-features which is expected to impact most of the clay macro-behaviour appears to be dominated not only by the electrostatic, electromagnetic and chemical inter-particle forces, but also by the mechanical interactions of the particle aggregates (either the stacks or the flocculated aggregates; Figure 3e) which recur in the micro-REV. In the following, it will be shown how these aggregates evolve and how, at the same time, the overall micro-REV fabric changes under different η compressions.

4. Clays under study

4.1 Composition

The index properties of the clays of reference in the paper are plotted in the plasticity and activity charts in Figure 4; their mineralogical composition is also reported. Their behaviour when reconstituted in the laboratory is discussed in the paper, whereas details about their natural state and history will be provided in the companion paper, where their micro to macro behaviour will be also discussed.

4.2 Clay states and macro-behaviour in compression

Figure 5 reports data resulting from laboratory 1D compression on the reconstituted clays in Figure 4, normalized for composition using the void index $I_v = (e\text{-}e^*_{100})/(e^*_{100}\text{-}e^*_{1000})$ (Burland, 1990).

While the post-mortem micro-analyses for the clay states in Figure 5 allow for insight into the evolution of reconstituted clay microstructure in 1D compression, evidence of the microstructure variations activated by changes in η has been acquired through post-mortem micro-analyses of reconstituted Lucera and Gulf of Guinea clays subjected to different constant η compressions.

Mitaritonna et al. (2014) report results of such micro-analyses for reconstituted Lucera clay. This had been 1D normally compressed from slurry to $\sigma'_v = 100$ kPa ($I_v = 0$) in the consolidometer, before further constant η compression in the stress path (Figure 6), where, for this clay, 1D compression corresponds to η = 0.6. As shown in Figure 6, η was set to range from 0 to 0.8 in the stress path testing, during which the evolution of clay stiffness anisotropy, in terms of ratio G_{hh}/G_{hv}, was measured by means of bender element tests, as discussed by the authors.

In particular, the specimens were subjected to η = 0, 0.3, 0.6 in Tests 1, 2, 3 respectively, and to η = 0.8 in both Tests 4 and 5 (Figure 6). The state paths followed by the

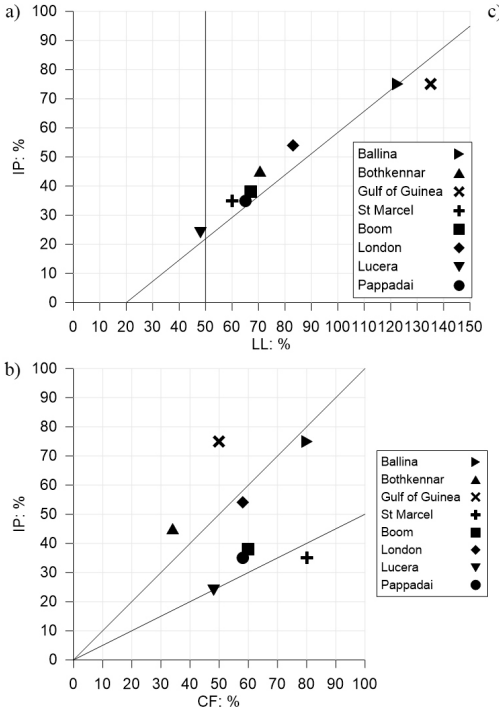

c)

Clay	Mineralogy*
soft clays	
Bothkennar (Bot) *Hight et al. (1992); Smith et al. (1992); Tanaka et al. (2003)*	I; K; Qz; Fd †
Gulf of Guinea (GoG) *Hattab et al. (2013)*	K: 50; S: 15-25 †
St Marcel (StM) *Delage and Lefebvre (1984)*	Ch: 4-16; I: 2-10; V: 2-9 ‡
Ballina (Ba) *Pineda et al. (2016a, b)*	K: 2,3–24,5; I: 7,8–23,3; Qz: 8,8–55,9; I/S: 9,5-20,1; amorphous minerals: 1,7–22,4; Pl: 2,9–15,2; Py: 0–6,4; K-Fd: 1,2–5,5; Mca: 0,9–2,1; Ca: 0–1 ‡
stiff clays	
Pappadai (Pa) *Cotecchia and Chandler (1997; 2000), Cotecchia et al. (2019), Guglielmi (2018)*	I: 20; Ch: 14; S: 12; K: 12; I/S: 10 ‡
Lucera (Lu) *Mitaritonna (2006), Guglielmi (2018)*	I/S: 77 (40-45); K: 9; I: 8; Ch: 6 †
Boom (Bo) *Belanteur et al. (1997), Delage et al. (2007), Lima et al. (2008), Della vecchia et al. (2011)*	I: 50; S: 30; I/S+K: 10 †
London *Gasparre et al. (2007)*	I: 21-38; K: 11-15; Ch; S; M ‡
Brown Weathered London (BWL) *Skempton and Jones (1944), Monroy et al. (2010)*	-

*Percentages are shown, when available, otherwise the minerals are listed in descending order of dominance: I, illite; K, kaolinite; Ch, chlorite; S, smectite; I/S, mixed-layers illite/smectite (illite % within parentheses); V, vermiculite; M, montmorillonite; Q, quartz; Fd, feldspar; Ca, carbonate; Pl, plagioclase; Py, pyrite, Mca, mica.
† % of the fraction ≤2 μm.
‡ % of the bulk sample.

Figure 4. (a) Plasticity chart, (b) activity chart and (c) mineralogy of the clays analysed in the lecture (after Guglielmi et al., 2024; data after Bishop et al., 1965; Burland, 1990; Cotecchia & Chandler, 2000; Delage & Lefebvre, 1984; Hattab & Fleureau, 2010; Smith, 1992; Pineda et al., 2016a).

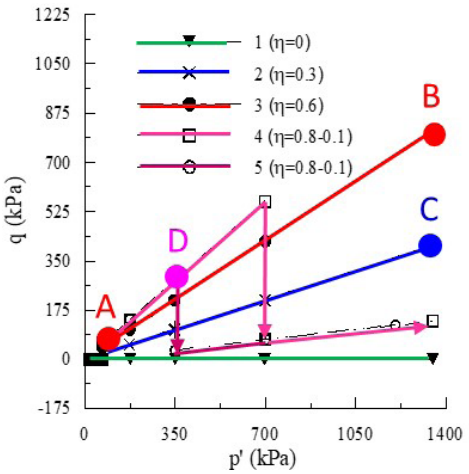

Figure 6. Results of constant-η compression tests in the *q-p'* plane (adapted after Mitaritonna et al., 2014).

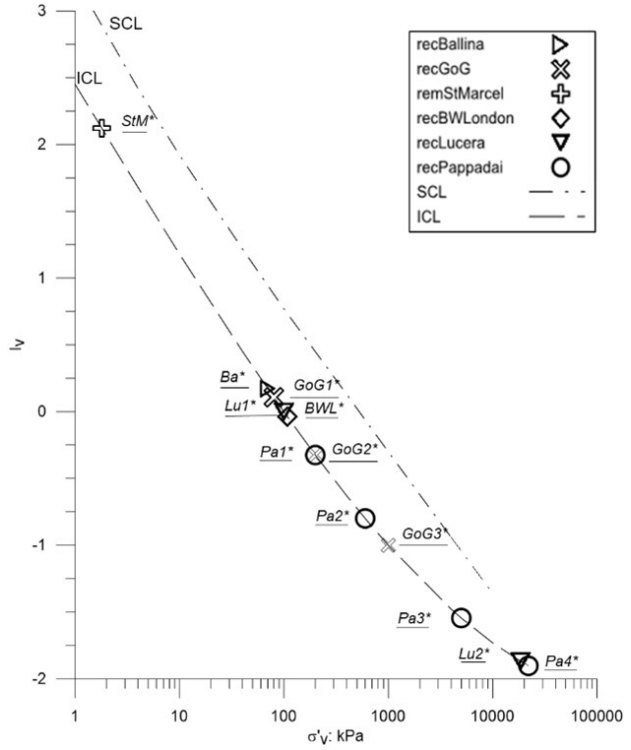

Figure 5. Reconstituted clays in Figure 4: 1D normally consolidated states subjected to micro-analyses (data after Bishop et al., 1965; Burland, 1990; Cotecchia & Chandler, 1997 and 1998; Cotecchia et al., 2019; Delage & Lefebvre, 1984; Hattab et al., 2013; Smith, 1992; Monroy et al., 2010; Pineda et al., 2016a, b; Cotecchia et al., 2019; Guglielmi et al., 2024). ICL: intrinsic compression line; SCL: sedimentation compression line (Burland, 1990).

specimens in the compression plane: specific volume, *v*, versus log *p'*, are reported in Mitaritonna et al. (2014)[5]. The roughly parallel normal consolidation lines, NCLs, followed by the clay state in different η compressions confirm the shift to the right of the NCL for decreasing η. Also, the data show the shift of the clay state from one ηNCL to the other while undergoing a variation in η (Tests 4 and 5). The reconstituted clay fabric was investigated before and after stress path testing (states shown in Figure 6), by means of SEM analyses and digital image processing; the corresponding microscale data are recalled in the following section.

5. Reconstituted clay microstructure at different stages of 1D compression

Figure 7 shows SEM micrographs taken from Delage & Lefebvre (1984), Pineda et al. (2016b) and Hattab et al. (2013) on vertical fractures of the clay specimens of $I_v > 0$ in Figure 5; these micrographs are analysed herein to provide knowledge on the microstructure of such clays, with the purpose to build a conceptual model. The SEM micrographs in Figures 7a and b refer to state StM* of St Marcel clay, the least plastic of the soft clays of reference (Figure 4). The micrographs of the higher plasticity clays (Figure 4), Ballina and Gulf of Guinea clay, at states Ba* and GoG1* respectively in Figure 5, are shown in Figures 7c, d and e. The void ratios of all the specimens investigated in Figure 7 are high and very close (see the void ratios indicated in the figure), but the I_v value of StM* is highest (Figure 5), due to the much lower liquid limit of this clay of high content in rock flour.

For all the three clay specimens, of $I_v > 0$, the fabric is found to be formed of flocculated aggregates of particles and domains (e.g., card-house to bookhouse aggregation; first sketch in Figure 3e). The randomness in particle orientation holds from the large to the medium scale (recognizable at the different magnifications, Figure 7). In the higher activity clay specimens Ba* and GoG1*, a spatial variability in the density of packing of the flocculated particles and domains is recognized, since densely flocculated aggregates are recognizable, within which the intra-aggregate porosity is formed by hardly detectable pores, much smaller than the pores between the aggregates, which appear to be connected by domains acting as bridges. Such inter-aggregate pores are about 1 μm in size (Figure 7). Such variability in density of the flocculated packing across the whole fabric is more evident in the higher activity Ba* and GoG1* specimens, than in the low activity StM* specimen.

It follows that the micro-REV fabric of all three specimens at $I_v > 0$ is classifiable as random (low average orientation; Delage & Lefebvre, 1984; Pineda et al., 2016b; Hattab et al., 2013), as typical for card-house to bookhouse fabric classes (Sides and Barden 1971). Especially for the higher plasticity clays (Ba* and GoG*), the fabric appears to match the honeycomb sub-class (Sides & Barden, 1971; Collins & McGown, 1974), sketched in Figure 7f modified after Griffiths & Joshi (1990). Honeycomb fabric features had been already recognised for a high-water content reconstituted kaolin ($e \approx 2{*}e_{wL}$) at an early stage of compression by

[5] See Figure 4 in Mitaritonna et al. (2014).

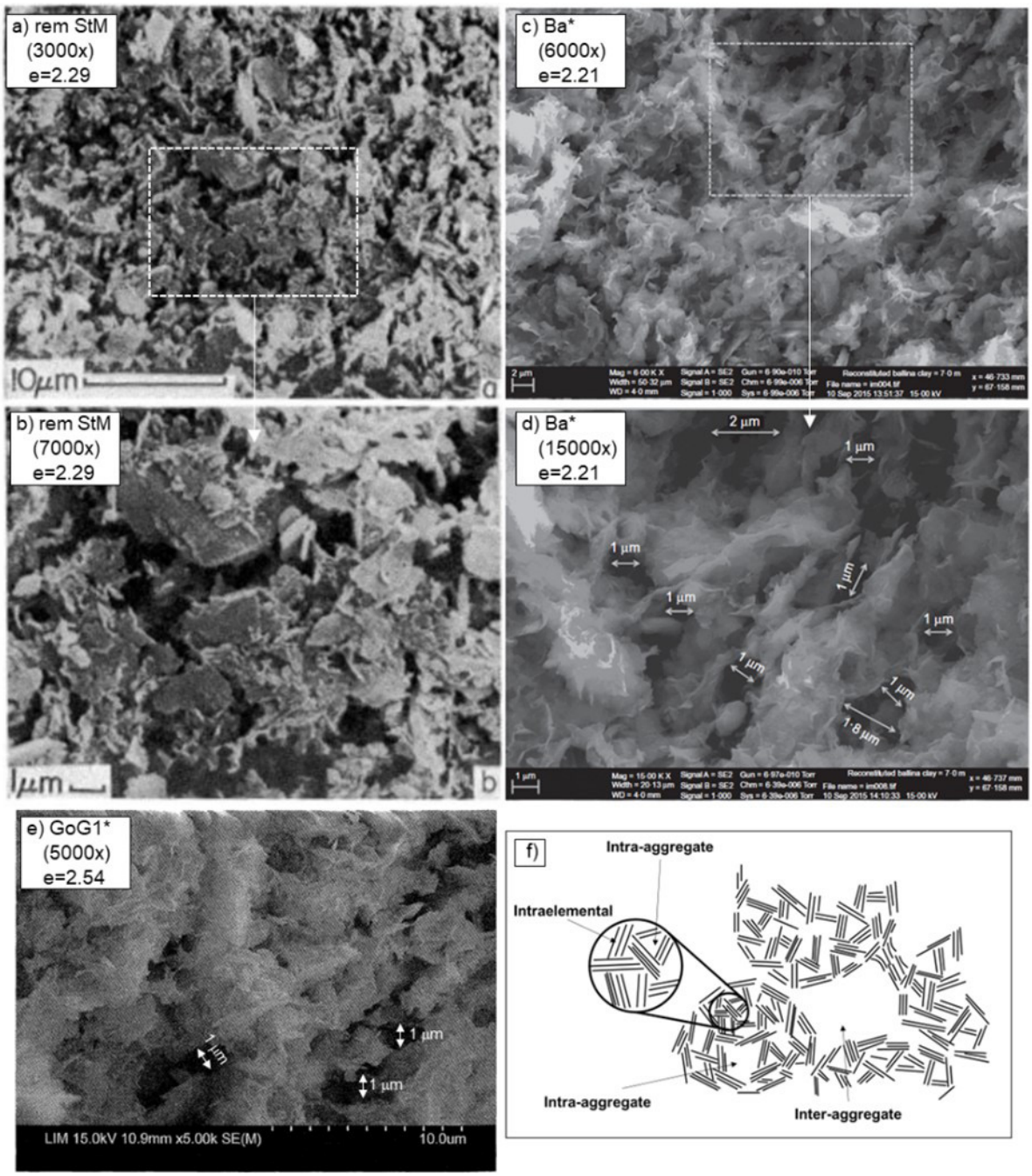

Figure 7. SEM micrographs corresponding to the clays states in Figure 5: StM* - a, b; Ba* - c, d; GoG1* - e. Sketch of honeycomb fabric (f) modified after Griffiths & Joshi (1990). Sources of the micrographs: Delage & Lefebvre (1984); Pineda et al. (2016b); Hattab et al. (2013).

Cotecchia et al. (1982) (see Guglielmi et al., 2024), and for an illitic clay slurry at the liquid limit by Griffiths & Joshi (1990), who distinguished: the smallest pores within either the domains, or the most tightly aggregated floccules, as intra-elemental (Figure 7f); the relatively higher pores within the flocculated aggregates as inter-group (intra-aggregate in the following); the larger pores confined by the aggregates and the bridges as inter-assemblage (inter-aggregate in the following).

The porosity features detected through the SEM investigation are confirmed by the MIP data in Figure 8 (data from Guglielmi, 2018). Both the high activity Ba* and GoG1* specimens include a bimodal pore size distribution, PSD, with a large dominant pore size (DPS) for the inter-aggregate porosity, around 900 nm for Ba* and 1250 nm for GoG1*, and a DPS around 60 nm for the intra-aggregate porosity. For StM*, instead, the PSD curve (replotted from Delage & Lefebvre 1984) is characterized by a single DPS around 444

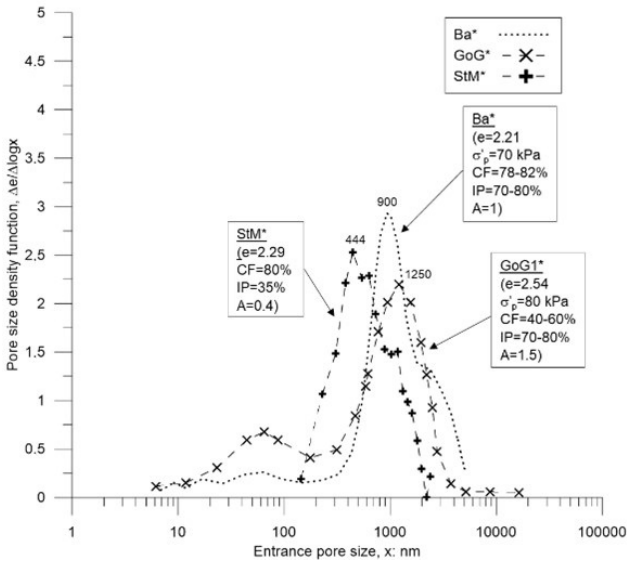

Figure 8. Comparison of PSD curves for StM*, GoG1* and Ba* in Figure 5 (data from Delage & Lefebvre, 1984; Hattab et al., 2013; Pineda et al., 2016b; modified after Guglielmi et al., 2024).

nm and by significant pore volume distributed across the pore sizes, both below and above the DPS (the latter representing inter-aggregate pores). Therefore, the PSD curves in Figure 8 suggest an influence of the activity index A on the PSD of the flocculated clay, with a possible shift from a mono-modal to a bi-modal PSD with increasing A. However, Yu et al. (2016) recognized a bimodal PSD for a kaolin slurry (i.e., a low activity clay) reconstituted at $2*w_L$ and consolidated to σ'_v = 50 kPa. Hence, the influence of composition and boundary conditions on the tendency of low plasticity clays to acquire either a mono-modal, or a bi-modal PSD at early stages of compression needs further investigation.

The previous micro-scale data have been compared with those obtained for the reconstituted specimens 1D compressed to higher pressures in Figure 5. The results of SEM analyses carried out on reconstituted Lucera clay (of activity close to that of StM*), Lu1*, consolidated to e = 0.92 and $I_v \approx 0$ (Figure 5), are shown in Figure 9. The micrographs reveal typical features of a compressed bookhouse fabric (Sides & Barden, 1971). The image processing indicates, for both the micro-REV micrographs

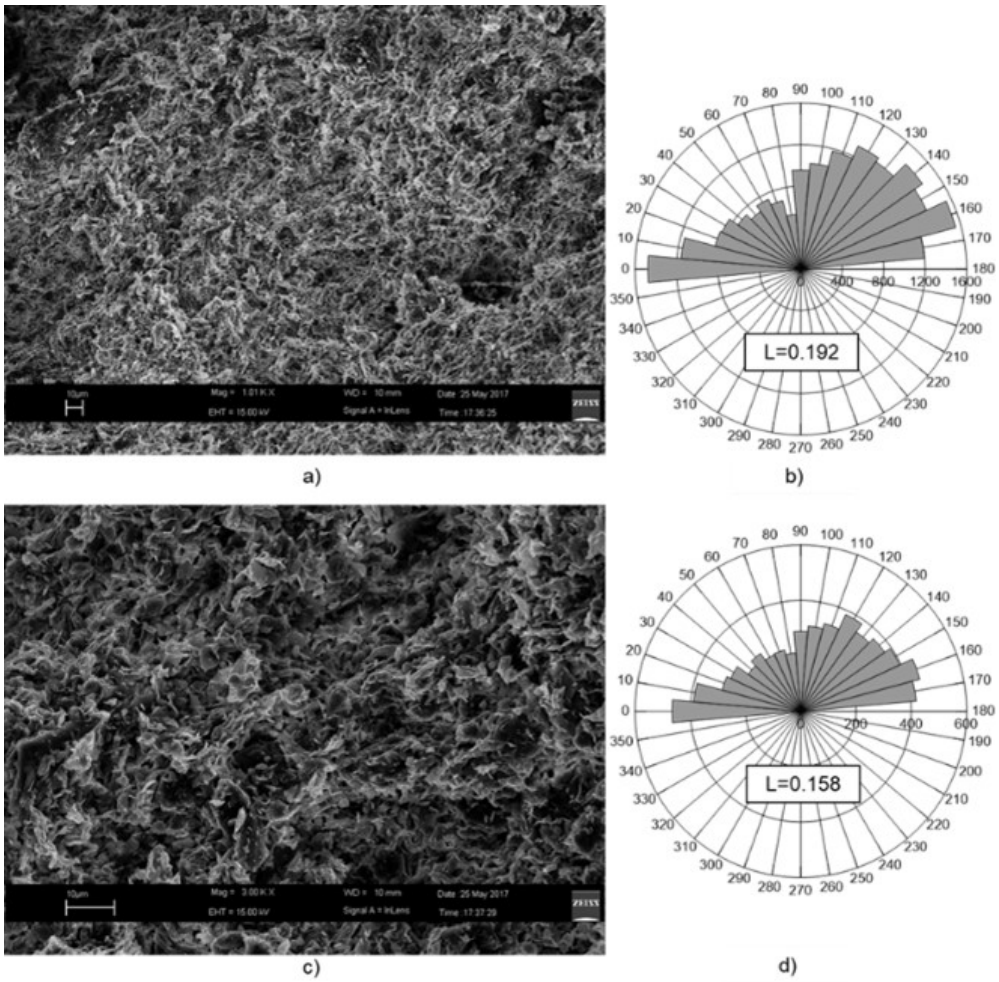

Figure 9. (a, c) FESEM micro-REV micrographs of Lu1* in Figure 5 and (b, d) corresponding direction histograms and indices of fabric orientation (modified after Guglielmi et al., 2024).

in Figure 9, a low orientation degree, since the index of fabric orientation does not reach $L = 0.21$. Hence, the data indicate that the 1D compression of the reconstituted clay to $I_v \approx 0$ increases the fabric orientation, but it does not yet generate a highly oriented fabric by this stage of compression. However, Cotecchia et al. (2019, 2020) found that for reconstituted Pappadai clay, of slightly higher plasticity and activity than Lucera clay (Figure 4), compression to I_v slightly beyond 0, as for Pa1* in Figures 2 and 5, results in a well-oriented micro-REV fabric, characterized by an index of fabric orientation $L = 0{\cdot}23$ - $0{\cdot}27$ (e.g., Figure 3c). In this case, the fabric matches a repetitive alternation of long sub-horizontal stacks, of highly oriented particles (Figure 3e), and aggregates of randomly oriented particles/domains in edge to face contact (see §3 and Cotecchia et al., 2019, 2020 for other micrographs). On the whole, the 1D compression of the clay beyond $I_v = 0$ (e.g. from Lu1* to Pa1*) seems to determine a fabric evolution exemplified in Figure 3d: sub-horizontal stacks form across the random fabric, as originally sketched by Sfondrini (1975) (Figure 3d-i); thereafter, additional stacks form and the first ones thicken, as sketched in Figure 3d-ii. The image processing provides quantitative evidence that the degree of orientation of the micro-REV fabric of reconstituted clays is initially very low, but increases through 1D compression and can become high ($L \geq 0.21$) early beyond $I_v = 0$ ($\sigma'_v > 100$ kPa). However, the degree of orientation of the clay fabric is far from uniform across the micro-REV of $L \geq 0.21$; conversely, as observed at large scale (§3), it is very high within the stacks and low in the flocculated fabric preserved between the stacks.

Figure 10 shows the PSD curves of Pa1* and Lu1* (Figure 5) and the PSD function obtained by Monroy et al. (2010) for reconstituted brown weathered London clay (Figure 4), BWL* in Figure 5, whose fabric is characterized by a recognizable degree of orientation as well (Monroy et al., 2010). Lu1* is characterized by a less regular PSD than both Pa1* and BWL*, with a larger DPS ≈ 1000 nm, probably as a result of both its slightly coarser composition and the less oriented fabric, achieved by $I_v \approx 0$. The other two specimens, of similar CF, A and high degree of orientation, embody a markedly mono-modal PSD, with a DPS < 1 μm, in the range of the micro-porosity (Matsuo & Kamon, 1977), and a limited macro-porosity, distributed over a wide range of entrance pore sizes (data from Guglielmi, 2018; Guglielmi et al., 2018). The slightly higher value of DPS of BWL* may be due to its lower compression with respect to Pa1*. On the whole, with 1D compression the increase in the degree of fabric orientation is found to be accompanied by the onset of a more regular and monomodal pore size distribution, as well as a reduction in the DPS (Figure 10). The DPS tends to correspond to the porosity present within the stacks, as recognized by Guglielmi et al. (2024) through the micrograph inspections. Hence, these results enhance the previous knowledge about the changes in PSD of clays under 1D compression (Delage & Lefebvre, 1984; Lapierre et al., 1990; Tanaka & Locat, 1999; Hattab & Fleureau, 2010; Hattab et al., 2013), indicating that both the inter-aggregate and the intra-aggregate porosity change with compression.

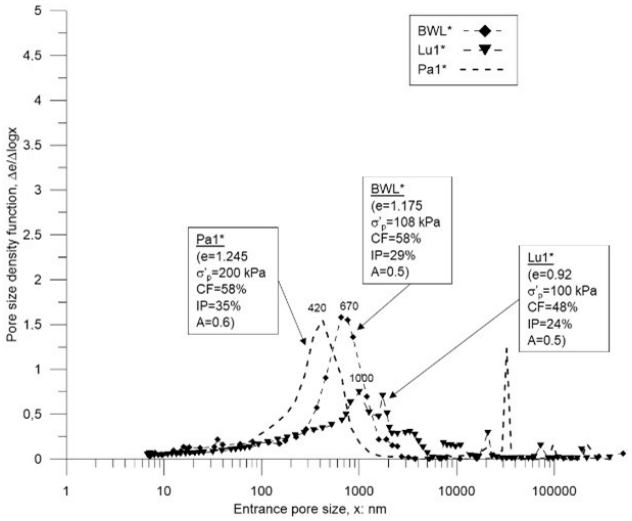

Figure 10. Comparison of PSD curves for Pa1*, Lu1* and BWL*, after compression in consolidometer (data for London clay after Monroy et al., 2010; modified after Guglielmi et al., 2024).

While all the micro-scale data discussed above refer to reconstituted clay specimens at the end of compression in the consolidometer, further fabric evolution in 1D compression has been investigated through micro-analyses on clay specimens of GoG*, Pa* and Lu* compressed to higher pressures in the oedometer (GoG1*, GoG2* and GoG3*; Lu1* and Lu2*; Pa1*, Pa2*, Pa3* and Pa4*, Figure 5).

The PSD (Figure 11a) and SEM data for both GoG2* (σ'_v = 200 kPa) and GoG3* (σ'_v = 1000 kPa) have been reported by Hattab et al. (2013). These confirm that 1D compression reduces the inter-aggregate DPS both in size and frequency, while the medium scale orientation of the particles increases (Hattab et al., 2013). An increase in fabric orientation is observed also by Hicher et al. (2000) based upon SEM micrographs of both kaolinite and bentonite slurry compressed to 1 MPa and ≈ 6 MPa, respectively.

1D compression of Lu*, from Lu1* at $I_v \approx 0$, to very high pressure, Lu2*, is found to change the initial irregular PSD curve of Lu1* into a neat monomodal curve (Figure 11b), with an intra-aggregate DPS which undergoes a major decrease with compression to high pressure. Therefore, the data confirm that compression first causes the collapse of the inter-aggregate porosity, but further on it causes the reduction in size of the intra-aggregate DPS. Since the DPS occurs within the stacks (Guglielmi et al., 2024), 1D compression to high pressures is found to cause volumetric straining of the stacks.

Figure 11c shows that the compression of Pa* from Pa1* to Pa2* and Pa3* at high pressures (Figure 5), also causes the shift of the DPS towards lower pore sizes, i.e., reduction of the intra-aggregate pore sizes.

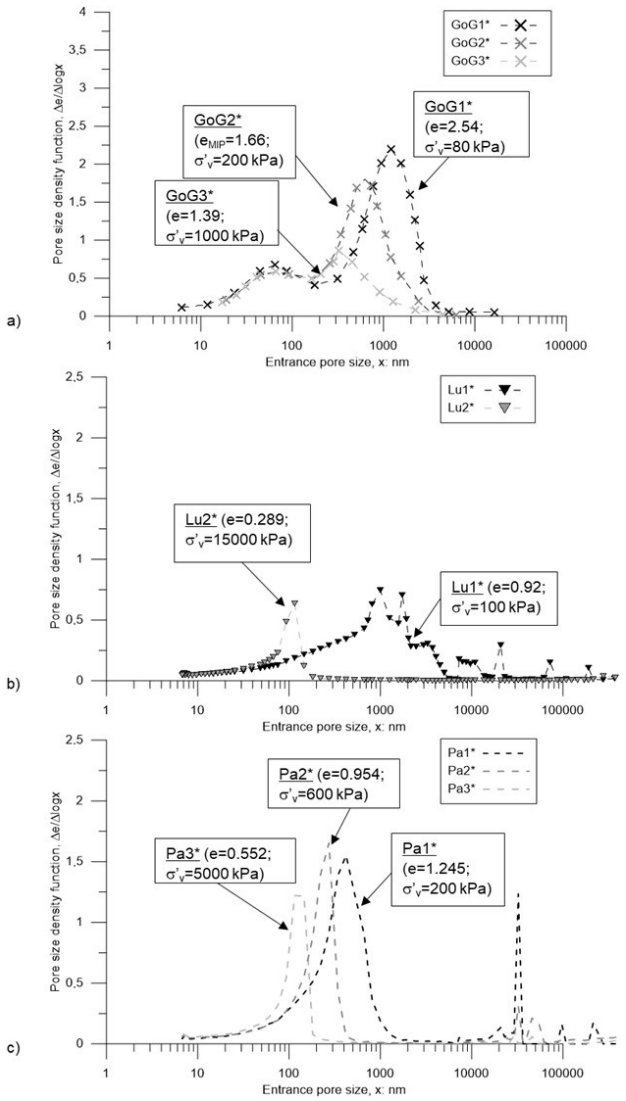

Figure 11. Evolution in 1D compression of PSD curves of reconstituted clays: Gulf of Guinea (a), Lucera (b) and Pappadai (c) (states in Figure 5; data from Guglielmi, 2018; modified after Guglielmi et al., 2024).

Furthermore, Cotecchia et al. (2019) also show that Pa* clay fabric compressed from Pa1* to Pa4* at σ'_v = 22 MPa (Figure 5), is characterized by an index of micro-REV fabric orientation L = 0.24 (Figure 12), which is about that measured for specimen Pa1*. Hence, 1D compression is found to determine the onset of a high degree of micro-REV fabric orientation quite early beyond I_v = 0, but its continuation up to high pressure does not determine any significant further increase in such orientation degree, which is found to remain constant.

This observation is consistent with the recognition that the particle orientation does not become ubiquitous through 1D compression, since layers of bookhouse fabric are found preserved even at very large pressures, as shown in Figure 12, sketched in Figure 3d-*ii* and discussed by Guglielmi et al. (2024). All the changes in

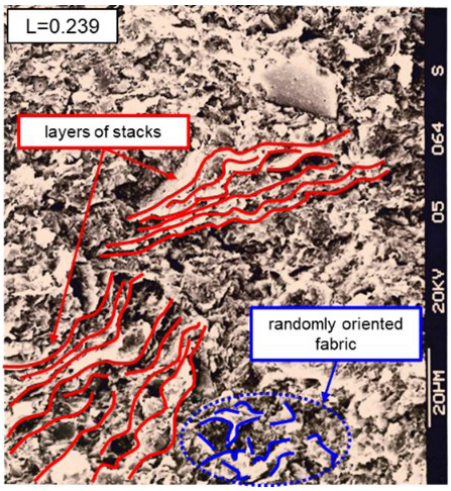

Figure 12. Compressed reconstituted Pappadai clay, Pa4* (Figures 2 and 5): medium magnification micrograph (with examples of different local fabric arrangements) and index of fabric orientation (modified after Cotecchia et al., 2019).

reconstituted clay fabric and PSD characterized through the data presented above are synthesized in the framework shown in Figure 13.

6. Compressions at different stress ratios, η

Figure 14 shows SEM micrographs resulting from the micro-scale investigation programme performed on reconstituted Lucera clay and quoted in §4.2, which has been extensively presented by Mitaritonna et al. (2014). The micrographs refer to clay specimens subjected to the different constant η compressions shown in Figure 6 and, for each of them, the figure shows also the direction histograms resulting from image processing and the corresponding index of fabric orientation L.

The SEM micrographs are representative of many others acquired in the investigation of the medium scale fabric features of the clay, i.e. of the micro-REV clay fabric, after loading to the stress states A, B, C and D in Figure 6. In particular: A refers to the state of the reconstituted clay 1D consolidated (η = 0.6) to σ'_v = 100 kPa in the consolidometer; B to the state achieved by the same clay when, after 1D consolidation to state A, is further 1D compressed (constant η = 0.6) up to p' = 1400 kPa; C to the state of the clay, initially consolidated to state A, and thereafter compressed at constant η = 0.3 up to p' = 1400 kPa; D to the state of the clay initially consolidated to state A, and thereafter compressed at constant η = 0.8 up to p' = 350 kPa.

The SEM data for both specimens A and B (Figures 14 a and b) confirm that the micro-REV fabric achieved in 1D compression to $I_v \geq 0$ is formed of sub-horizontal stacks of domains inter-layered with trusses of domains (bookhouse-like), as sketched in Figure 13; hence this fabric is not uniform at the large scale. Also, the direction histograms corresponding to states A and B confirm that the index of fabric orientation, L, becomes

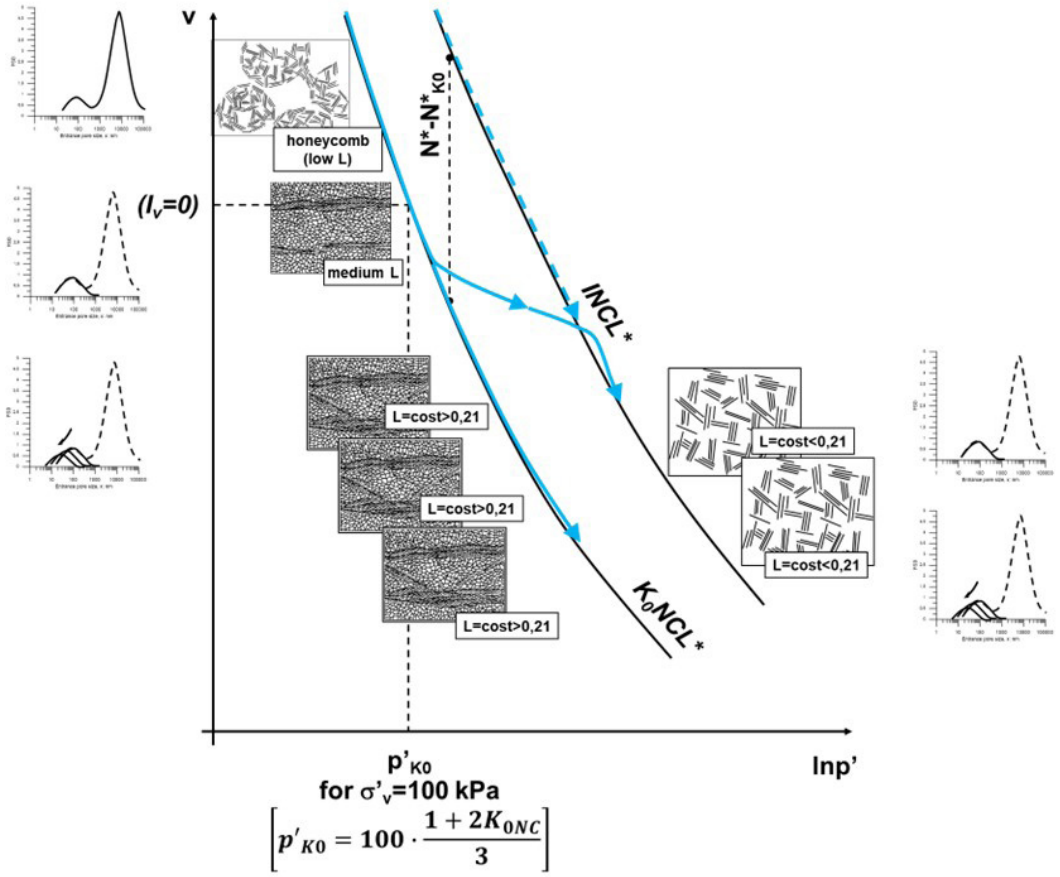

Figure 13. Schematic framework of the evolution in microstructure of reconstituted clay subjected to 1D and isotropic compression.

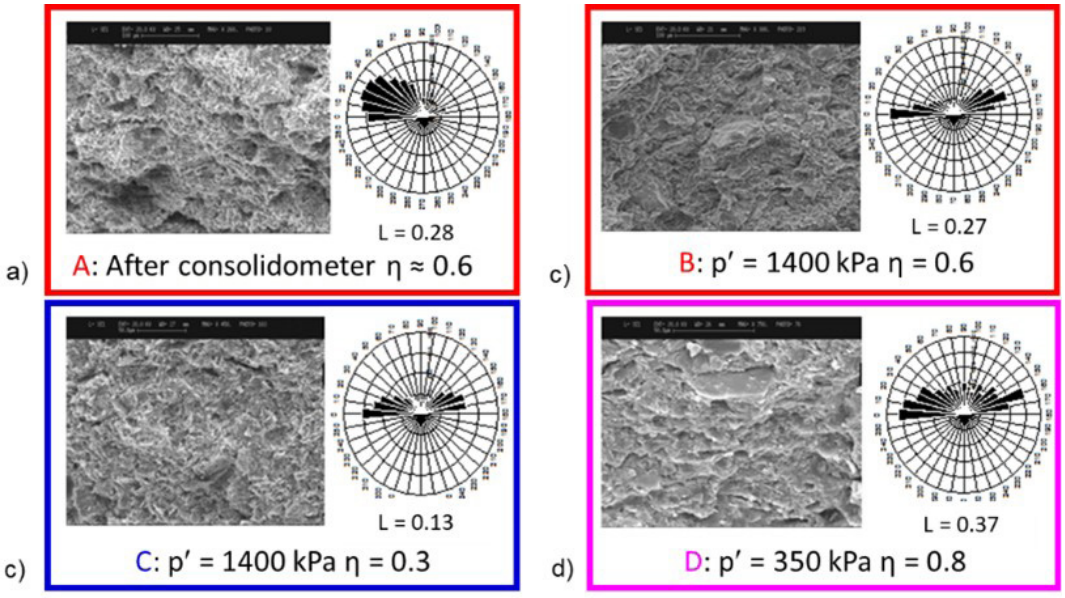

Figure 14. Micro-REV fabric of reconstituted Lucera clay after different η compression tests and corresponding direction histograms and indices of fabric orientation (Mitaritonna et al., 2014).

high in 1D compression by $I_v = 0$, or slightly beyond (in this case about 0.28), and that further yielding of the clay in 1D compression to high pressure does not increase such degree of orientation. The micro-scale observations achieved for the clay

fabric after different constant η compressions beyond gross yield, instead, show that the fabric features change with η.

Figure 14c shows that the initially oriented fabric, corresponding to state A in Figure 6 (Figure 14a), experiences a severe rearrangement into a far less oriented one when brought to yield and further normally compressed at η = 0.3 up to p' = 1400kPa, as demonstrated by the drop in L to ≈ 0.13 for state C in Figure 6 (Figure 14c). Such a drop in L makes the fabric in C be classified as random (Martinez-Nistal et al., 1999). Instead, Figure 14d shows that the oriented fabric at state A experiences an accelerated increase in fabric orientation when further compressed under η = 0.8, so that the index of fabric orientation L attains a very high value, 0.37, at p' = 350kPa (state D in Figure 6).

It is worth highlighting that the data from Mitaritonna et al. (2014) portray the change in fabric orientation that can be achieved by a medium density reconstituted clay (1D compressed to p' ≈ 70 kPa), through a three times increase of p' imposed at a constant η different from the initial one. Consistent results have been achieved by Hattab & Fleureau (2010) for initially 1D consolidated reconstituted kaolinite, which is found to achieve a more random fabric through isotropic compression to a p' over 12 times the initial one. The behaviour of reconstituted kaolinite under isotropic compression was also investigated by Hicher et al. (2000), who found that the increase of p' of about 3 times in isotropic conditions generates a rather isotropic particle orientation for an initially oriented fabric. Sivakumar et al. (2002), instead, claim that kaolin specimens consolidated isotropically from slurry to p' = 500 kPa retain evidence of an anisotropic microstructure; however, this may be due to the far larger pressures which are required to generate a change in fabric degree of orientation by changing η. The different micro-REV fabrics found to be achieved by reconstituted clays under different constant η compressions are sketched, for η_{K0} and η_0, in Figure 13. Further micro-scale investigations are still required to assess the reconstituted fabric changes over small p' increases after the change in η.

Data are available also about the PSD changes taking place in the clay when moving from a constant ηNCL to another one. Hattab et al. (2013) report microstructural analyses of reconstituted GoG clay after isotropic compression starting from state GoG1* (Figure 5). Figure 15 (data from Guglielmi, 2018) shows the PSD changes occurring with isotropic compression to GoG^*_{iso}, by comparison with the PSD changes achieved through 1D compression to GoG3* (Figure 5). For the two specimens, compressed from the same initial state, the volumetric strain ε_{vol} induced by further compression is calculated by Hattab et al. (2013) and reported in the figure. A mild bimodal PSD is still preserved in the 1D compressed state GoG3*. Conversely, despite the volumetric strain in either the isotropic (ε_{vol} = 30%) or the 1D (ε_{vol} = 32%) compression being almost the same, a larger change in PSD is observed in the isotropic case, for which the inter-aggregate porosity is reduced, and the PSD changed from bimodal to monomodal. This PSD change is achieved despite micrographs of the isotropically compressed specimen revealing that fabric orientation is still locally preserved.

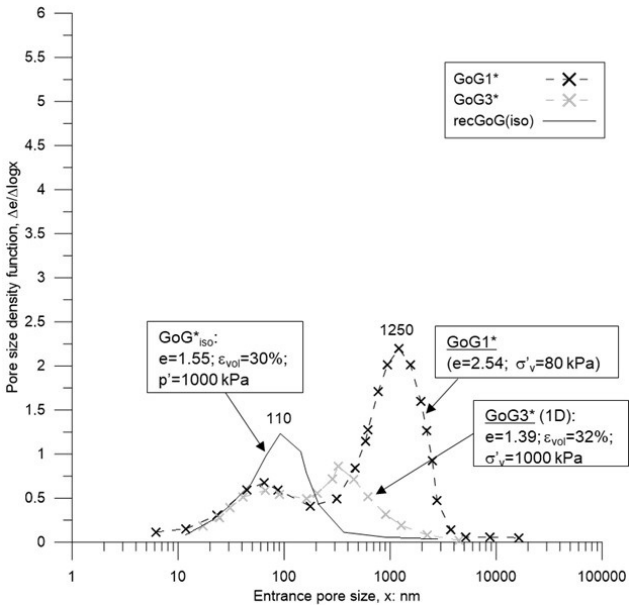

Figure 15. Comparison of PSD curves after isotropic (GoG^*_{iso}) and 1D compression (GoG1* and GoG3*) for reconstituted GoG clay (states GoG1* and GoG3* in Figure 5; data after Hattab et al., 2013); modified after Guglielmi et al. (2024).

7. Summary of the findings

From the above data the following findings can then be extracted:

- Medium-low to high activity clay particles, within a slurry settling at high I_v (> 0; liquidity index LI > 1) in 1D conditions, tend to aggregate according to a repetitive card-house to bookhouse mode (Figure 3e), with a separation between distinct aggregates, which results in a honeycomb fabric (Figure 7f), increasing the higher the clay activity index is. Hence, medium to high plasticity reconstituted clays achieve a low orientation micro-REV fabric, of honeycomb type (Figure 7f) at early stages of compression, with L << 0.2 and significant inter-aggregate porosity (major DPS ≈ 1μm). However, the PSD is bimodal for high plasticity clays, since the most active particles (e.g., the smectite fraction) allow for the presence of a far lower DPS within the aggregates, whereas this is not the case for the less active clays.
- When the clays are consolidated under 1D compression towards I_v ≈ 0 (σ'_v = 100 kPa), a progressive reduction of the inter-aggregate porosity of the honeycomb fabric and a reduction of the macro-porosity for either the overall card-house, or bookhouse, fabric of the less active clay occurs; in both cases the larger

pores, of size about 1μm, are reduced in size and the clay PSD heads towards a monomodal PSD, with DPS in the range of the hundreds of nm. Such a process is associated with an increase in the degree of orientation of the micro-REV fabric. This appears to result from the piling up of face-to-face contact particles, or domains (Figure 3e), within stacks, which tend to acquire a sub-horizontal orientation. For the originally honeycomb fabric, it can be observed that there are inter-aggregate bridges which first contribute to the collapse of the inter-aggregate porosity and which tend to adhere to the stacks. However, such a more orderly fabric is still of low average orientation by $I_v \approx 0$ (Figure 13).

- With increasing σ'_v, below $I_v \approx 0$ the micro-REV fabric achieves an increasing orientation degree at a rate dependent on the plasticity index. Further 1D compression generates further reorientation of particles, which coalesce with the stacks or form new ones, as sketched in Figure 3d-ii and Figure 13. Part of such an orientation process contributes to the thickening of the sub-horizontal stacks.
- Despite such an orientation process, original bookhouse fabric portions are preserved. Hence, the orientation of the particles under 1D compression is not at all ubiquitous, also for $I_v << 0$ (Figure 13). Evidently, the inter-particle forces within the preserved bookhouse portions, which are largely of either electrostatic, electromagnetic, or chemical nature, resist the mechanical action, so that these aggregates act as a whole mechanical fraction, undergoing straining (volumetric and shear), but keep the random fabric.
- At the same time, the achieved monomodal PSD of the clay undergoes an evolution characterized by a reduction in both the frequency and the size of the DPS, due to a reduction in porosity of the stacks and of the random fabric aggregates which are preserved (see sketch in Figure 13).
- Possibly further orientation of particles may occur with further 1D compression to high pressures, and the additional oriented particles are likely to adhere to and thicken the stacks (Figure 3d-ii). However, the micro-REV fabric orientation degree, *L*, is found to reach a threshold value and not increase above it. Such an important finding may be justified if a different deformability between the stacks and the flocculated fabric portions, preserved between the stacks, is accounted for. Indeed, the reduction in size of the intra-aggregate pores, occurring with 1D compression, may be expected to be higher within the stacks than within the bookhouse fabric portions, due to the higher inter-particle forces in the bookhouse fabric. Consequently, the straining of the stacks compensates their thickening due to further particle orientation and the proportion of the micro-REV fabric having a very high degree of orientation is not found to increase when inspecting the medium magnification micrographs (i.e., the ratio between the size of the stacks and the size of the bookhouse fabric portions in the medium scale fabric analyses remains reasonably constant).
- No micro-scale observations are available for the fabric changes generated by lower η compression (e.g., isotropic) of a reconstituted clay fabric 1D consolidated to $I_v > 0$. However, MIP data for high I_v clays compressed isotropically have shown that the reduction in η leads to a faster collapse of the inter-aggregate porosity with respect to higher η compressions. Indeed, a η decrease affects the inter-aggregate voids sooner.
- With regard to the fabric changes caused by different constant η compressions of a medium dense 1D consolidated clay, Mitaritonna et al. (2014) show that, starting from $I_v \approx 0$, the change in η results in significant variations in fabric orientation if the clay is compressed to medium-high pressures.

8. Preliminary conclusions about the modelling implications of the micro-scale data

The results discussed above represent a database useful for the progress of the research line b in Figure 1, aimed at the modelling of the micro-scale processes in clays for the prediction of their macro-response. In particular, since the findings summarized in §7 refer to reconstituted clays, they represent fabric settings which should be achieved through the micro-scale modelling for medium to high plasticity clays of stable bonding, as is the case for the clays sedimenting either in the laboratory consolidometer, or *in situ* in a high energy deposition environment. Furthermore, the clays should achieve initial consistency under initial 1D compression. Figure 13 reports the framework of the micro-scale findings of reference for such micro-scale modelling.

The micro-scale findings in §7 represent also a database useful for the research line *a* in Figure 1, aiming at relating the clay macro-behaviour predicted through constitutive laws formalized in the framework of continuum mechanics, to the micro-scale processes. In the following, some of the indications provided by the summarized findings are briefly discussed.

First, the fabric changes taking place in the clay when undergoing constant η compression (illustrated in Figure 13) provide reasons for the occurrence of the normal consolidation line of reconstituted clays under isotropic compression ($\eta = 0$), INCL*, to the right of that followed in 1D compression, K_0NCL*. In other words, the micro-scale observations justify why the intercept of the INCL*, N*, is higher than that of the K_0NCL*, N_{K0}*. It can be recognized that the less oriented fabric developing through isotropic gross yielding, within which

particles and domains are largely in edge to face contact, is consistent with a less deformable material under increasing *p'* than that embodying a more oriented fabric, such as that of the clay gross yielding in 1D compression. As a matter of fact, the edge to face inter-particle forces of the less oriented fabric developing with isotropic yielding, resists more the external mechanical actions (more limited straining) than the face to face forces within the stacks present in the 1D compressed clay. It can be argued that the smaller the difference in fabric between the clay subjected to isotropic gross yielding and that subjected to 1D gross yielding, the smaller is the difference [N* - N*$_{K0}$].

Mitaritonna et al. (2014) provide evidence that the high degree of orientation that the reconstituted clay achieves through 1D compression gives rise to directional properties at the macro-scale. They report measurements of the elastic stiffness anisotropy ratio, G_{hh}/G_{hv}, of reconstituted Lucera clay achieved by means of T-shape horizontal bender element tests (Dyvik & Madshus, 1985; Pennington et al., 1997; Mitaritonna et al., 2010), performed all the way through the tests shown in Figure 6. The values of G_{hh}/G_{hv} measured during the radial stress paths in Figure 6 are plotted versus *p'* in Figure 16. It can be seen that in 1D compression, at η = 0.6, a constant stiffness anisotropy ratio G_{hh}/G_{hv} = 1.12-1.13 (Figure 16) is found to correspond to the constant degree of fabric anisotropy assessed through the micro-scale investigations (Figures 14a, b). Hence, the steady orientation degree, *L*, measured during the η = 0.6 compression is consistent with the constant value of the anisotropy degree G_{hh}/G_{hv} = 1.11 recorded at the macro-scale. Such finding confirms that the micro-REV fabric features, rather than the large-scale fabric features, control the clay macro-behaviour and that the elastic anisotropy of the clay is generated by the high degree of orientation of the micro-REV fabric, irrespective of the local poorly oriented fabric aggregates present in the highly oriented medium scale fabric. Furthermore, Mitaritonna et al. (2014) find that the elastic stiffness ratios either decrease, or increase, depending on the imposed stress ratio η (Figure 16), and reach different constant G_{hh}/G_{hv} values at *p'* about four times the initial one (*p'* = 70 kPa).

These observations indicate that the clay has to be compressed well beyond gross-yield in order to acquire constant directional properties which, evidently, depend on the achieved constant degree of micro-REV fabric orientation, *L*, which in turn depends on η. In particular, compression paths at η lower than the initial η = 0.6 (η=0, or 0.3), induce a permanent reduction in the degree of elastic anisotropy, leading to $G_{hh}/G_{hv} \approx 1.05$ for η = 0.3 and about 1.01 for η = 0. The isotropic loading to high pressures appears almost to erase the initial directional properties of the clay. In contrast, the elastic anisotropy ratio increases up to 1.22 in the clay compressed at η = 0.8. Also, the data show that a change in degree of shear stiffness anisotropy requires significant plastic straining, as a small amount of

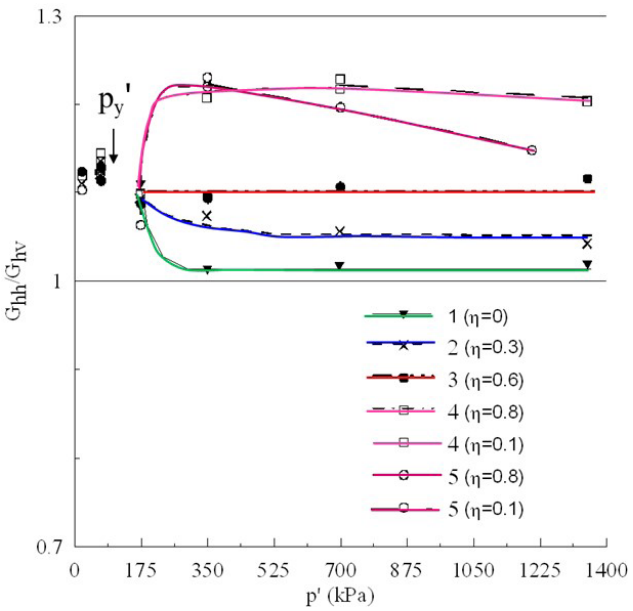

Figure 16. Anisotropy ratio G_{hh}/G_{hv} plotted against mean effective stress for different η compression tests (modified after Mitaritonna et al., 2014).

irreversible deformation under the new η is not sufficient to modify the previously acquired directional property to a significant extent.

Mitaritonna et al. (2014) report, for reconstituted Lucera clay, the plot of G_{hh}/G_{hv} – η,[6] along with the corresponding *L* values. The corresponding plot relating the degree of micro-REV fabric orientation, *L*, achieved through the constant η compressions is shown in Figure 17a. Accordingly, Figure 17b formalizes a monotonic increase in G_{hh}/G_{hv} with *L*, evidence of the dependency of the elastic cross-anisotropy of the clay on the micro-REV degree of orientation. Therefore, the research results show that the directional elasto-plastic coupling made evident by the plot in Figure 16 is due to the micro-REV fabric changes taking place in the clay with gross yielding, as shown by the relation between G_{hh}/G_{hv} and the microfabric constitutive parameter $L(\varepsilon_{ij}^{P})$ in Figure 17b.

Since the data validate the dependency of the variation in elastic anisotropy ratio on the variation in fabric orientation at the micro-REV scale (Figure 17b), the observation that the elastic anisotropy ratio varies slowly after the change in compression stress ratio η, shown in Figure 16, in turn suggests that the variation in the degree of fabric orientation, *L*, takes place slowly after the change in η. It may be envisaged a chaotic fabric change taking place soon after η variation, followed by a progressive fabric evolution heading towards a new constant fabric orientation, *L* (Figure 17b). At the same time, the MIP data discussed in §6 suggest that the change in η impacts sooner the PSD (faster for isotropic

[6] See Figure 14 in Mitaritonna et al. (2014).

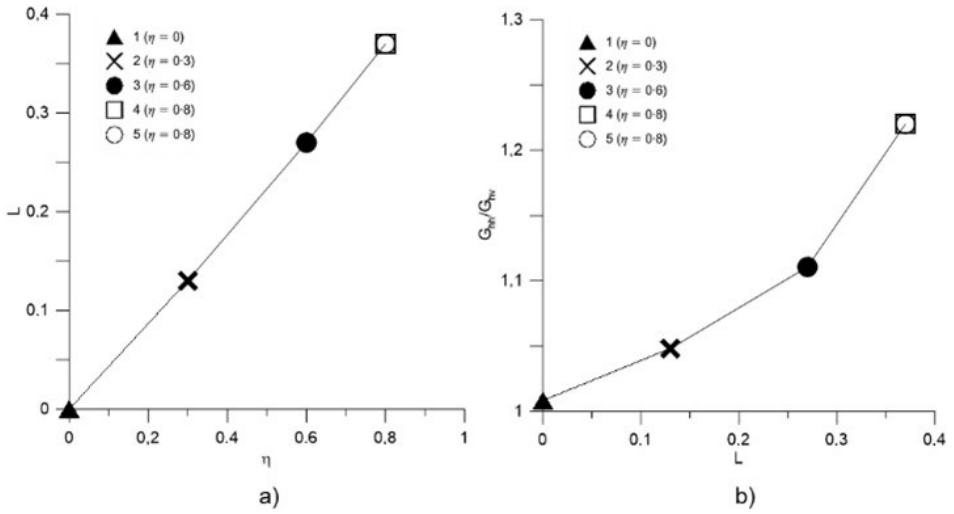

Figure 17. Anisotropy ratio G_{hh}/G_{hv} against: stress ratio η (a) and micro-REV orientation index L (b).

compression versus 1D compression) than the micro-REV fabric orientation, L. The findings concerning the micro-REV fabric orientation degree and the PSD features for each constant η compression of the clay at $I_v < 0$, i.e.: $L(\eta)$ reached in constant η compression after a significant amount of plastic straining at constant η, and the monomodal PSD with reducing DPS, are schematized in Figure 13.

The findings sketched in Figure 13 can be of reference in the selection of new microfabric constitutive variables for clays of stable bonding, like the reconstituted clays, to be implemented in advanced constitutive laws accounting for the micro-scale processes which determine the clay macro-behaviour (research line a-ii in Figure 1; e.g., Rollo & Amorosi, 2022). In particular, useful microfabric constitutive parameters appear to be: the micro-REV fabric orientation index, $L(\eta)$, or $L(\varepsilon_{ij}^{P})$ if accounting for the transient stages of evolution of L; the corresponding angle of orientation $\theta(\varepsilon_{ij}^{P})$; the PSD function and the DPS(ε_{ij}^{P}) function.

Meanwhile, still concerning the research line a-*i* in Figure 1, the steady degree of fabric orientation, L, and the monomodal PSD characterizing the micro-REV fabric of reconstituted clays during plastic straining under constant η compression (Figure 13), justify the success of the normalization for volume (through $p_e^*(e)$) of the shear response of reconstituted clay specimens all compressed along the same radial stress paths (constant η; e.g., Figure 6). Such a response is exemplified in Figure 18. The micro-scale data show that, when the clay undergoes constant η compression from $I_v \approx 0$ to $I_v << 0$, its micro-REV fabric reaches soon a stage in which the only fabric feature undergoing major changes with constant η compression is the DPS of a monomodal PSD, since L and θ remain constant. This occurs for any η (Figure 13). Therefore, the reduction in clay void ratio, e, with no significant change in L is the possible reason why e is the main internal variable of the plastic hardening of

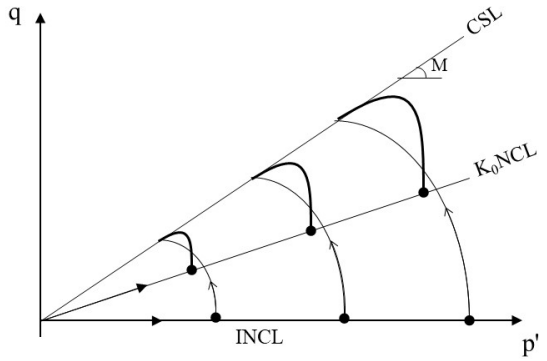

Figure 18. Schematic representation of undrained shear paths after different η compressions.

reconstituted clays (Rendulic, 1936; Roscoe et al., 1958; Henkel, 1956) and isotropic volumetric hardening applies when yielding takes place under constant η (e.g., the Cam Clay models; Schofield & Wroth (1968); Roscoe & Burland (1968); Figure 18).

However, since the steady degree of micro-REV fabric orientation reached at constant η varies with η, the differences in clay stiffness and stiffness anisotropy among the specimens compressed at different constant η make their stress-strain response to shearing vary with η. It may be envisaged that the higher is the variation of L with changing η, the less the shear response of the clay complies with the Rendulic principle[7]. Accordingly, it is likely that the Rendulic principle, i.e., the successful normalization by $p_e^*(= e^{[(N^*-V)/\lambda^*]})$ of the stress paths of specimens sheared after different η compressions, suits the shearing behaviour only of a family of specimens, including

[7] For instance, the reader is referred to the normalization by p^*_e of shear paths of either isotropically or 1D consolidated specimens of reconstituted Pappadai clay, as shown by Cotecchia et al. (2011) in their Figure 20.

1D compressed specimens and specimens isotropically compressed, for which compression has not been such as to determine significant variation in fabric orientation, *L*.

However, reaching a common critical state at the end of shearing of specimens compressed under different η is justified by the major fabric changes caused by shearing to large strains, which causes very high degrees of fabric orientation (function $L(\eta)$; see *L* values for high η), irrespective of the original consolidation fabric (Guglielmi et al., in press).

Declaration of interest

The authors have no conflicts of interest to declare. All co-authors have observed and affirmed the contents of the paper and there is no financial interest to report.

Authors' contributions

Federica Cotecchia: conceptualization, methodology, validation, writing - reviewing and editing. Simona Guglielmi: conceptualization, investigation, data curation, validation, writing - reviewing and editing. Francesco Cafaro: investigation, validation, reviewing. Antonio Gens: supervision, validation, reviewing & editing.

Data availability

The datasets generated analyzed in the course of the current study are available from the corresponding author upon request.

List of symbols and abbreviations

DPS	dominant pore size
G_{hh}/G_{hv}	elastic stiffness anisotropy ratio
I_v	void index
e	void ratio
e_{wL}	void ratio at liquid limit
w	water content
A	clay activity
C_s	swelling index
C_s^*/C_s	swell sensitivity
CF	clay fraction
ICL	intrinsic compression line
L	index of fabric orientation
w_L	liquid limit
MIP	mercury intrusion porosimetry
OCR	overconsolidation ratio σ'_p / σ'_v
w_P	plastic limit
PSD	pore size density function
S_σ	stress sensitivity
S_r	degree of saturation
SCL	sedimentation compression line
SEM	scanning electron microscopy
YSR	yield stress ratio σ'_y / σ'_v
η	stress ratio
σ^*_e	equivalent vertical effective stress on the ICL
σ'_p	vertical (geological) preconsolidation pressure
σ'_v	vertical effective stress
σ'_y	vertical effective stress at yield

References

Alder, B.J., & Wainwright, T.E. (1959). Studies in molecular dynamics. I. General method. *The Journal of Chemical Physics*, 31(2), 459-466. http://dx.doi.org/10.1063/1.1730376.

Anandarajah, A. (1994). Discrete element method for simulating behaviour of cohesive soils. *Journal of Geotechnical Engineering*, 120(9), 1593-1613. http://dx.doi.org/10.1061/(ASCE)0733-9410(1994)120:9(1593).

Anandarajah, A. (2000). Numerical simulation of one-dimensional behaviour of a kaolinite. *Geotechnique*, 50(5), 509-519. http://dx.doi.org/10.1680/geot.2000.50.5.509.

Andò, E., Viggiani, G., Hall, S.A., & Desrues, J. (2013). Experimental micro-mechanics of granular media studied by x-ray tomography: recent results and challenges. *Géotechnique Letters*, 3(3), 142-146. http://dx.doi.org/10.1680/geolett.13.00036.

Bandera, S., O'Sullivan, C., Angioletti-Uberti, S., & Tangney, P., (2019). An evaluation of contact models for particle-scale simulation of clay. *E3S Web of Conferences*, 92, 14001. http://dx.doi.org/10.1051/e3sconf/20199214001.

Bandera, S., O'Sullivan, C., Tangney, P., & Angioletti-Uberti, S. (2021). Coarse-grained molecular dynamics simulations of clay compression. *Computers and Geotechnics*, 138, 104333. http://dx.doi.org/10.1016/j.compgeo.2021.104333.

Baudet, B.A., & Stallebrass, S.E. (2004). A constitutive model for structured clays. *Geotechnique*, 54(4), 269-278. http://dx.doi.org/10.1680/geot.2004.54.4.269.

Birmpilis, G., Ahmadi-Naghadeh, R., & Dijkstra, J. (2019). Macroscopic interpretation of nano-scale scattering data in clay. *Géotechnique Letters*, 9(4), 355-360. http://dx.doi.org/10.1680/jgele.18.00241.

Birmpilis, G., Mohammadi, A., Villanova, J., Boller, E., Ando, E., & Dijkstra, J. (2022a). Fabric investigation of natural sensitive clay from 3D nano- and microtomography data. *Journal of Engineering Mechanics*, 148(2), 04021151. http://dx.doi.org/10.1061/(ASCE)EM.1943-7889.0002044.

Birmpilis, G., Andò, E., Stamati, O., Hall, S.A., Gerolymatou, E., & Dijkstra, J. (2022b). Experimental quantification of 3D deformations in sensitive clay during stress-probing. *Geotechnique*, 73(8), 655-666. http://dx.doi.org/10.1680/jgeot.21.00114.

Bishop, A.W., Webb, D.L., & Lewin, P.I. (1965). Undisturbed samples of London Clay from Ashford Common shaft:

strength-effective stress relationship. *Geotechnique*, 15(1), 1-31. http://dx.doi.org/10.1680/geot.1965.15.1.1.

Bjerrum, L. (1967). Engineering geology of Norwegian normally-consolidated marine clays as related to settlements of buildings. *Geotechnique*, 17(2), 81-117. http://dx.doi.org/10.1680/geot.1967.17.2.83.

Borja, R.I., Tamagnini, C., & Amorosi, A. (1997). Coupling plasticity and energy-conserving elasticity models for clays. *Journal of Geotechnical and Geoenvironmental Engineering*, 123(10), 948-957. http://dx.doi.org/10.1061/(ASCE)1090-0241(1997)123:10(948).

Burland, J.B. (1990). On the compressibility and shear strength of natural soils. *Geotechnique*, 40(3), 329-378. http://dx.doi.org/10.1680/geot.1990.40.3.329.

Cafaro, F., & Cotecchia, F. (2001). Structure degradation and changes in the mechanical behaviour of a stiff clay due to weathering. *Geotechnique*, 51(5), 441-453. http://dx.doi.org/10.1680/geot.2001.51.5.441.

Cetin, H. (2004). Soil-particle and pore orientations during consolidation of cohesive soils. *Engineering Geology*, 73(1-2), 1-11. http://dx.doi.org/10.1016/j.enggeo.2003.11.006.

Chapman, D.L. (1913). A contribution to the theory of electrocapillarity. *The London, Edinburgh and Dublin Philosophical Magazine and Journal of Science*, 25(6), 475-481. http://dx.doi.org/10.1080/14786440408634187.

Collins, K., & McGown, A. (1974). The form and function of microfabric features in a variety of natural soils. *Geotechnique*, 24(2), 223-254. http://dx.doi.org/10.1680/geot.1974.24.2.223.

Cotecchia, V., Federico, A., & Trizzino, R. (1982). Microtessiture di sedimenti argillosi. Esperimenti su kaolinite e bentonite ed esempi di sedimenti argillosi dell'Italia Meridionale. *Geologia Applicata e Idrogeologia*, 17, 53-78 (in Italian).

Cotecchia, F., & Chandler, R.J. (1995). The geotechnical properties of the Pleistocene clays of the Pappadai valley. *Quarterly Journal of Engineering Geology*, 28(1), 5-22. http://dx.doi.org/10.1144/GSL.QJEGH.1995.028.P1.02.

Cotecchia, F. (1996). *The effects of structure on the properties of an Italian Pleistocene clay* [PhD thesis]. University of London, London.

Cotecchia, F., & Chandler, R.J. (1997). The influence of structure on the pre-failure behaviour of a natural clay. *Geotechnique*, 47(3), 523-544. http://dx.doi.org/10.1680/geot.1997.47.3.523.

Cotecchia, F., & Chandler, R.J. (1998). One-dimensional compression of a natural clay: structural changes and mechanical effects. In A. Evangelista & L. Picarelli (Eds.), *Proceedings of the 2nd International Symposium on Hard Soils Soft Rocks* (pp. 103-114). Rotterdam: Balkema.

Cotecchia, F., & Chandler, R.J. (2000). A general framework for the mechanical behaviour of clays. *Geotechnique*, 50(4), 431-447. http://dx.doi.org/10.1680/geot.2000.50.4.431.

Cotecchia, F., Mitaritonna, G., & Vitone, C. (2011). Investigating the influence of microstructure, loading history and fissuring on the clay response. In *Proceedings of the International Symposium on Deformation Characteristics of Geomaterials*, Seoul, Korea.

Cotecchia, F., Cafaro, F., & Guglielmi, S. (2016). Microstructural changes in clays generated by compression explored by means of SEM and image processing. *Procedia Engineering*, 158, 57-62. http://dx.doi.org/10.1016/j.proeng.2016.08.405.

Cotecchia, F., Guglielmi, S., Cafaro, F., & Gens, A. (2019). Characterisation of the multi-scale fabric features of high plasticity clays. *Géotechnique Letters*, 9(4), 361-368. http://dx.doi.org/10.1680/jgele.18.00230.

Cotecchia, F., Guglielmi, S., & Gens, A. (2020). Investigation of the evolution of clay microstructure under different loading paths and impact on constitutive modelling. *Global Journal of Engineering Sciences*, 5(1), 000603. http://dx.doi.org/10.33552/GJES.2020.05.000603.

Cuisinier, O., & Laloui, L. (2004). Fabric evolution during hydromechanical loading of a compacted silt. *International Journal for Numerical and Analytical Methods in Geomechanics*, 28(6), 483-499. http://dx.doi.org/10.1002/nag.348.

Cundall, P.A., & Strack, O.D.L. (1979). A discrete numerical model for granular assemblies. *Geotechnique*, 29(1), 47-65. http://dx.doi.org/10.1680/geot.1979.29.1.47.

Deirieh, A., Chang, I.Y., Whittaker, M.L., Weigand, S., Keane, D., Rix, J., Germaine, J.T., Joester, D., & Flemings, P.B. (2018). Particle arrangements in clay slurries: the case against the honeycomb structure. *Applied Clay Science*, 152, 166-172. http://dx.doi.org/10.1016/j.clay.2017.11.010.

Delage, P., & Lefebvre, G. (1984). Study of the structure of a sensitive Champlain clay and of its evolution during consolidation. *Canadian Geotechnical Journal*, 21(1), 21-35. http://dx.doi.org/10.1139/t84-003.

Delage, P., & Pellerin, M. (1984). Influence de la lyophilisation sur la structure d'une argile sensible du Quebec. *Clay Minerals*, 19(2), 151-160 (in French). http://dx.doi.org/10.1180/claymin.1984.019.2.03.

Delage, P. (2010). A microstructure approach to the sensitivity and compressibility of some Eastern Canada sensitive clays. *Geotechnique*, 60(5), 353-368. http://dx.doi.org/10.1680/geot.2010.60.5.353.

Derjaguin, B.V., & Landau, L. (1941). Theory of the stability of strongly charged lyophobic sols and the adhesion of strongly charged particles in solutions of electrolyte. *Acta Physicochimica*, 14, 633-662.

Desrues, J., Viggiani, G., & Besuelle, P. (2010). *Advances in X-ray tomography for geomaterials*. New York: John Wiley & Sons.

Diamond, S. (1970). Pore size distribution in clays. *Clays and Clay Minerals*, 18(1), 7-23. http://dx.doi.org/10.1346/CCMN.1970.0180103.

Dyvik, R., & Madshus, C. (1985). Laboratory measurements of Gmax using bender elements. In *Proceedings of the ASCE Annual Convention: Advances in the Art of Testing Soils Under Cyclic Conditions*, Detroit, Michigan.

Ebrahimi, D., Pellenq, R.J.M., & Whittle, A.J. (2012). Nanoscale elastic properties of montmorillonite upon water adsorption. *Langmuir*, 28(49), 16855-16863. PMid:23181550. http://dx.doi.org/10.1021/la302997g.

Ebrahimi, D., Pellenq, R.J.M., & Whittle, A.J. (2016). Mesoscale simulation of clay aggregate formation and mechanical properties. *Granular Matter*, 18(3), 49. http://dx.doi.org/10.1007/s10035-016-0655-8.

Ebrahimi, D., Whittle, A.J., & Pellenq, R.J.M. (2014). Mesoscale properties of clay aggregates from potential of mean force representation of interactions between nanoplatelets. *The Journal of Chemical Physics*, 140(15), 154309. PMid:25338898. http://dx.doi.org/10.1063/1.4870932.

Frenkel, D., & Smit, B. (2013). *Understanding molecular simulation*. Orlando: Academic Press.

Gasparre, A., Nishimura, S., Coop, M.R., & Jardine, R.J. (2007). The influence of structure on the behaviour of London Clay. *Geotechnique*, 57(1), 19-31. http://dx.doi.org/10.1680/geot.2007.57.1.19.

Gay, J.G., & Berne, B.J. (1981). Modification of the overlap potential to mimic a linear site potential. *The Journal of Chemical Physics*, 74(6), 3316-3319. http://dx.doi.org/10.1063/1.441483.

Gens, A., & Nova, R. (1993). Conceptual bases for a constitutive model for bonded soil and weak rocks. In *Proceedings of the International Conference on Hard Soils - Soft Rocks* (pp. 483-494), Athens.

Gens, A., & Potts, D.M. (1988). Critical state models in computational geomechanics. *Engineering Computations*, 5(3), 178-197. http://dx.doi.org/10.1108/eb023736.

Gillott, J.E. (1970). Fabric of Leda clay investigated by optical, electron-optical, and X-ray diffraction methods. *Engineering Geology*, 4(2), 133-153. http://dx.doi.org/10.1016/0013-7952(70)90009-8.

Gillott, J.E. (1973). Methods of sample preparation for microstructural analysis of soil. In G.K. Rutherford (Ed.), *Soil Microscopy: Proceedings of the 4th International Working Meeting Soil Micromorphology* (Vol. 1, pp. 143-164), Kingston, Ontario, Canada. Limestone Press.

Gouy, G. (1910). Sur la constitution de la charge electrique a la surface d'un electrolyte. *Journal de Physique Théorique et Appliquée*, 9(1), 457-468. http://dx.doi.org/10.1051/jphystap:019100090045700.

Griffiths, F.J., & Joshi, R.C. (1990). Clay fabric response to consolidation. *Applied Clay Science*, 5(1), 37-66. http://dx.doi.org/10.1016/0169-1317(90)90005-A.

Guglielmi, S. (2018). *Evolution of the clay micro-structure in compression and shearing loading paths* [PhD thesis]. Polytechnic University of Bari, Bari, Italy.

Guglielmi, S., Cotecchia, F., Cafaro, F., & Gens, A. (2018). Microstructural changes underlying the macro-response of a stiff clay. In P. Giovine, P. M. Mariano & G. Mortara (Eds.), *Micro to MACRO mathematical modelling in soil mechanics, trends in mathematics* (pp. 89-97). Basel: Springer Nature. http://dx.doi.org/10.1007/978-3-319-99474-1_9.

Guglielmi, S., Cotecchia, F., Cafaro, F., Gens, A., Leroueil, S., Hight, D.W., & Locat, J. (2023). Discussion on analysis of the micro to macro response of clays to compression. *Geotechnique*. In press. http://dx.doi.org/10.1680/jgeot.22.D.006.

Guglielmi, S., Cotecchia, F., Cafaro, F., & Gens, A. (2024). Analysis of the micro to macro response of clays to compression. *Geotechnique*, 74(2), 134-154. http://dx.doi.org/10.1680/jgeot.21.00233.

Guida, G., Casini, F., Viggiani, G.M.B., Andò, E., & Viggiani, G. (2018). Breakage mechanisms of highly porous particles in 1D compression revealed by X-ray tomography. *Géotechnique Letters*, 8(2), 155-160. http://dx.doi.org/10.1680/jgele.18.00035.

Gupta, V., Hampton, M.A., Stokes, J.R., Nguyen, A.V., & Miller, J.D. (2011). Particle interactions in kaolinite suspensions and corresponding aggregate structures. *Journal of Colloid and Interface Science*, 359(1), 95-103. PMid:21489550. http://dx.doi.org/10.1016/j.jcis.2011.03.043.

Hall, S.A., Bornert, M., Desrues, J., Pannier, Y., Lenoir, N., Viggiani, G., & Bésuelle, P. (2010). Discrete and continuum analysis of localized deformation in sand using X-ray μCT and volumetric digital image correlation. *Geotechnique*, 60(5), 315-322. http://dx.doi.org/10.1680/geot.2010.60.5.315.

Hattab, M., & Fleureau, J.M. (2010). Experimental study of kaolin particle orientation mechanism. *Geotechnique*, 60(5), 323-331. http://dx.doi.org/10.1680/geot.2010.60.5.323.

Hattab, M., Hammad, T., Fleureau, J.M., & Hicher, P.Y. (2013). Behaviour of a sensitive marine sediment: microstructural investigation. *Geotechnique*, 63(1), 71-84. http://dx.doi.org/10.1680/geot.10.P.104.

Henkel, D.J. (1956). The effect of overconsolidation on the behaviour of clays during shear. *Geotechnique*, 6(4), 139-150. http://dx.doi.org/10.1680/geot.1956.6.4.139.

Hicher, P.Y., Wahyudi, H., & Tessier, D. (2000). Microstructural analysis of inherent and induced anisotropy in clay. *Mechanics of Cohesive-Frictional Materials*, 5(5), 341-371. http://dx.doi.org/10.1002/1099-1484(200007)5:5<341::AID-CFM99>3.0.CO;2-C.

Hight, D.W., Bond, A.J., & Legge, J.D. (1992). Characterization of the Bothkennar clay: an overview. *Geotechnique*, 42(2), 303-347. http://dx.doi.org/10.1680/geot.1992.42.2.303.

Israelachvili, J. (2011). *Intermolecular and surface forces* (3rd ed.). Amsterdam: Elsevier.

Jia, R., Lei, H., & Li, K. (2020). Compressibility and microstructure evolution of different reconstituted clays during 1D compression. *International Journal of Geomechanics*, 20(10), 04020181. http://dx.doi.org/10.1061/(ASCE)GM.1943-5622.0001830.

Kavvadas, M., & Amorosi, A. (2000). A constitutive model for structured soils. *Geotechnique*, 50(3), 263-273. http://dx.doi.org/10.1680/geot.2000.50.3.263.

Knabe, T., Datcheva, M., Lahmer, T., Cotecchia, F., & Schanz, T. (2013). Identification of constitutive parameters of soil using an optimization strategy and statistical analysis. *Computers and Geotechnics*, 49, 143-157. http://dx.doi.org/10.1016/j.compgeo.2012.10.002.

La Ragione, L., & Jenkins, J.T. (2007). The initial response of an idealized granular material. *Proceedings - Royal Society. Mathematical, Physical and Engineering Sciences*, 463(2079), 735-758. http://dx.doi.org/10.1098/rspa.2006.1792.

Lambe, T.W., & Whitman, R.V. (1969). *Soil mechanics*. New York: Wiley.

Lapierre, C., Leroueil, S., & Locat, J. (1990). Mercury intrusion and permeability of Louisville clay. *Canadian Geotechnical Journal*, 27(6), 761-773. http://dx.doi.org/10.1139/t90-090.

Leroueil, S., & Vaughan, P.R. (1990). The general and congruent effects of structure in natural soils and weak rocks. *Geotechnique*, 40(3), 467-488. http://dx.doi.org/10.1680/geot.1990.40.3.467.

Li, X., & Li, X.-S. (2009). Micro-macro quantification of the internal structure of granular materials. *Journal of Engineering Mechanics*, 135(7), 641-656. http://dx.doi.org/10.1061/(ASCE)0733-9399(2009)135:7(641).

Lima, A., Romero, E., Pineda, J.A., & Gens, A. (2008). Low-strain shear modulus dependence on water content of a natural stiff clay. In *Anais do XIV Congresso Brasileiro de Mecânica dos Solos e Engenharia Geotécnica* (pp. 1763-1768), Curitiba, Brazil.

Liu, J., Lin, C.L., & Miller, J.D. (2015). Simulation of cluster formation from kaolinite suspensions. *International Journal of Mineral Processing*, 145, 38-47. http://dx.doi.org/10.1016/j.minpro.2015.07.004.

Locat, J. (1995). On the development of microstructure in collapsible soils: lessons from the study of recent sediments and artificial cementation. In E. Derbyshire, T. Dijkstra & I.J. Smalley (Eds.), *Genesis and properties of collapsible soils* (pp. 93-128). Dordrecht: Springer Science+Business Media. http://dx.doi.org/10.1007/978-94-011-0097-7_6.

Manzano, F.J., Lamas, F., & Azañón, J.M. (2023). Overconsolidated flysch-type clays. engineering considerations for the strait of Gibraltar tunnel project. *Soils and Rocks*, 46(1), e2023002222. http://dx.doi.org/10.28927/SR.2023.002222.

Martinez-Nistal, A., Veniale, F., Setti, M., & Cotecchia, F. (1999). A scanning electron microscopy image processing method for quantifying fabric orientation of clay geomaterials. *Applied Clay Science*, 14(4), 235-243. http://dx.doi.org/10.1016/S0169-1317(98)00055-6.

Matsuo, S., & Kamon, M. (1977). Microscopic study on deformation and strength of clays. In *Proceedings of the 9th ICSMFE* (Vol. 1, pp. 201-204), Tokyo. Tokyo: The Japanese Society of Soil Mechanics and Foundation Engineering.

Mitaritonna, G., Amorosi, A., & Cotecchia, F. (2010). Multidirectional Bender Elements measurements in the triaxial cell: equipment set up and signal interpretation. *Italian Geotechnical Journal*, 1, 50-69.

Mitaritonna, G., Amorosi, A., & Cotecchia, F. (2014). Experimental investigation of the evolution of elastic stiffness anisotropy in a clayey soil. *Geotechnique*, 64(6), 463-475. http://dx.doi.org/10.1680/geot.13.P.191.

Mitchell, J.K. (1976). *Fundamentals of soil behaviour*. New York: Wiley.

Mitchell, J.K., & Soga, K. (2005). *Fundamentals of soil behaviour* (3rd ed). Hoboken: John Wiley & Sons.

Monroy, R., Zdravkovic, L., & Ridley, A. (2010). Evolution of microstructure in compacted London Clay during wetting and loading. *Geotechnique*, 60(2), 105-119. http://dx.doi.org/10.1680/geot.8.P.125.

Nardelli, V., & Coop, M.R. (2019). The experimental contact behaviour of natural sands: normal and tangential loading. *Geotechnique*, 69(8), 672-686. http://dx.doi.org/10.1680/jgeot.17.P.167.

O'Brien, N.R., & Slatt, R.M. (1990). *Argillaceous rock atlas*. Berlin: Springer-Verlag. http://dx.doi.org/10.1007/978-1-4612-3422-7.

Oda, M. (1972). Initial fabric and their relations to mechanical properties of granular material. *Soil and Foundation*, 12(1), 17-36. http://dx.doi.org/10.3208/sandf1960.12.17.

Oda, M. (1993). Inherent and induced anisotropy in plasticity theory of granular soils. *Mechanics of Materials*, 16(1-2), 35-45. http://dx.doi.org/10.1016/0167-6636(93)90025-M.

Oda, M., Konishi, J., & Nemat-Nasser, S. (1980). Some experimentally based fundamental results on the mechanical behaviour of granular materials. *Geotechnique*, 30(4), 479-495. http://dx.doi.org/10.1680/geot.1980.30.4.479.

Oda, M., Nemat-Nasser, S., & Konishi, J. (1985). Stress induced anisotropy in granular masses. *Soil and Foundation*, 25(3), 85-97. http://dx.doi.org/10.3208/sandf1972.25.3_85.

Pagano, A.G., Magnanimo, V., Weinhart, T., & Tarantino, A. (2020). Exploring the micromechanics of nonactive clays via virtual DEM experiments. *Geotechnique*, 70(4), 303-316. http://dx.doi.org/10.1680/jgeot.18.P.060.

Pedrotti, M., & Tarantino, A. (2018). An experimental investigation into the micromechanics of non-active clays. *Geotechnique*, 68(8), 666-683. http://dx.doi.org/10.1680/jgeot.16.P.245.

Pennington, D.S., Nash, D.F.T., & Lings, M.L. (1997). Anisotropy of G0 shear stiffness in Gault Clay. *Geotechnique*, 47(3), 391-398. http://dx.doi.org/10.1680/geot.1997.47.3.391.

Penumadu, D., & Dean, J. (2000). Compressibility effect in evaluating the pore-size distribution of kaolin clay using mercury intrusion porosimetry. *Canadian Geotechnical Journal*, 37(2), 393-405. http://dx.doi.org/10.1139/t99-121.

Pineda, J.A., Suwal, L.P., Kelly, R.B., Bates, L., & Sloan, S.W. (2016a). Characterisation of Ballina clay. *Geotechnique*, 66(7), 556-577. http://dx.doi.org/10.1680/jgeot.15.P.181.

Pineda, J.A., Liu, X.F., & Sloan, S.W. (2016b). Effects of tube sampling in soft clay: a microstructural insight. *Geotechnique*, 66(12), 969-983. http://dx.doi.org/10.1680/jgeot.15.P.217.

Pusch, R. (1970). Microstructural changes in soft quick clay at failure. *Canadian Geotechnical Journal*, 7(1), 1-7. http://dx.doi.org/10.1139/t70-001.

Rendulic, L. (1936). Poronziffer und –porenwasserdruck in Tonen. *Bauingenieur*, 17, 559-564.

Rollo, F., & Amorosi, A. (2022). Isotropic and anisotropic elasto-plastic coupling in clays: a thermodynamic approach. *International Journal of Solids and Structures*, 248, 111668. http://dx.doi.org/10.1016/j.ijsolstr.2022.111668.

Romero, E., & Simms, P.H. (2008). Microstructure investigation in unsaturated soils: a review with special attention to contribution of mercury intrusion porosimetry and environmental scanning electron microscopy. *Geotechnical and Geological Engineering*, 26(6), 705-727. http://dx.doi.org/10.1007/s10706-008-9204-5.

Roscoe, K.H., Schofield, A.N., & Wroth, C.P. (1958). On the yielding of soils. *Geotechnique*, 8(1), 22-53. http://dx.doi.org/10.1680/geot.1958.8.1.22.

Roscoe, K.H., & Burland, J.B. (1968). On the generalized stressstrain behaviour of wet clay. In J. Heymann & F.A. Leckie (Eds.), *Engineering plasticity* (pp. 535-609). Cambridge: Cambridge University Press.

Rouainia, M., & Wood, D.M. (2000). A kinematic hardening constitutive model for natural clays with loss of structure. *Geotechnique*, 50(2), 153-164. http://dx.doi.org/10.1680/geot.2000.50.2.153.

Sasanian, S., & Newson, T.A. (2013). Use of mercury intrusion porosimetry for microstructural investigation of reconstituted clays at high water contents. *Engineering Geology*, 158, 15-22. http://dx.doi.org/10.1016/j.enggeo.2013.03.002.

Schmertmann, J.H. (1969). Swell sensitivity. *Geotechnique*, 19(4), 530-533. http://dx.doi.org/10.1680/geot.1969.19.4.530.

Schofield, A.N., & Wroth, C.P. (1968). *Critical state soil mechanics*. London: McGraw-Hill.

Sfondrini, G. (1975). Caratteristiche microtessiturali e microstrutturali di alcuni sedimenti argillosi connesse con la natura ed il tipo delle sollecitazioni subite. *Geologia Applicata e Idrogeologia*, 10, 300-320 (in Italian).

Sides, G., & Barden, L. (1971). The microstructure of dispersed and flocculated samples of kaolinite, illite and montmorillonite. *Canadian Geotechnical Journal*, 8(3), 391-399. http://dx.doi.org/10.1139/t71-041.

Sivakumar, V., Doran, I.J., & Graham, J. (2002). Particle orientation and its influence on the mechanical behaviour of isotropically consolidated reconstituted clay. *Engineering Geology*, 66(3–4), 197-209. http://dx.doi.org/10.1016/S0013-7952(02)00040-6.

Sjoblom, K.J. (2016). Coarse-grained molecular dynamics approach to simulating clay behavior. *Journal of Geotechnical and Geoenvironmental Engineering*, 142(2), 06015013. http://dx.doi.org/10.1061/(ASCE)GT.1943-5606.0001394.

Skempton, A.W., & Northey, R.D. (1952). The sensitivity of clays. *Geotechnique*, 3(1), 30-53. http://dx.doi.org/10.1680/geot.1952.3.1.30.

Skempton, A.W. (1970). The consolidation of clays by gravitational compaction. *Quarterly Journal of the Geological Society of London*, 125(1-4), 373-411. http://dx.doi.org/10.1144/gsjgs.125.1.0373.

Smart, P., & Tovey, N.K. (1981). *Electron microscopy of soil and sediments: examples*. Oxford: Oxford University Press.

Smith, P.R. (1992). *The behaviour of natural high compressibility clays with special reference to consolidation on soft ground* [PhD thesis]. University of London, London, UK.

Smith, P.R., Jardine, R.J., & Hight, D.W. (1992). On the yielding of Bothkennar clay. *Geotechnique*, 42(2), 257-274. http://dx.doi.org/10.1680/geot.1992.42.2.257.

Tanaka, H., & Locat, J. (1999). A microstructural investigation of Osaka Bay clay: the impact of microfossils on its mechanical behaviour. *Canadian Geotechnical Journal*, 36(3), 493-508. http://dx.doi.org/10.1139/t99-009.

Tavenas, F., Des Rosiers, J.P., Leroueil, S., La Rochelle, P., & Roy, M. (1979). The use of strain energy as a yield and creep criterion for lightly overconsolidated clays. *Geotechnique*, 29(3), 285-304. http://dx.doi.org/10.1680/geot.1979.29.3.285.

Tovey, N.K. (1973) Quantitative analysis of electron micrographs of soil structure. In G.R. Pusch (Ed.), *Proceedings of International Symposium on Soil Structure* (Vol. 1, pp. 50-57). Stockholm: Swedish Geotechnical Institute.

Tovey, N.K., & Wong, K.Y. (1973). The preparation of soils and other geological materials for the scanning electron microscope. In *Proceedings of the International Symposium on Soil Structure* (pp. 176-183), Gothenburg, Sweden.

Veniale, F., Martinez-Nistal, A., Setti, M., Duminuco, P., & Tortelli, M. (1993). Quantification of clayey soil fabric by SEM image processing. In *Proceedings of the 10th International Clay Conference AIPEA* (Abstract 136), Adelaide, Australia.

Veniale, F., Setti, M., Cotecchia, F., & Martinez-Nistal, A. (1995). Correlation between fabric and geotechnical properties of argillaceous geomaterials. In *Proceedings of Euroclay '95* (Abstract 29), Leuven, Belgium. Leuven: European Clay Groups Association.

Verwey, E.J.W., & Overbeek, J.T.G. (1948). *Theory of the stability of lyophobic colloids*. Amsterdam: Elsevier.

Viggiani, G., Andò, E., Takano, D., & Santamarina, J. (2015). Laboratory X-ray tomography: a valuable experimental tool for revealing processes in soils. *Geotechnical Testing Journal*, 38(1), 61-71. http://dx.doi.org/10.1520/GTJ20140060.

Wan, R., Guo, P., & Al-Mamun, M. (2005). Behaviour of granular material in relation to their fabric dependencies. *Soil and Foundation*, 45(2), 77-86. http://dx.doi.org/10.3208/sandf.45.2_77.

Yao, M., & Anandarajah, A. (2003). Three-dimensional discrete element method of analysis of clays. *Journal of Engineering Mechanics*, 129(6), 585-596. http://dx.doi.org/10.1061/(ASCE)0733-9399(2003)129:6(585).

Yu, C.Y., Chow, J.K., & Wang, Y.-H. (2016). Pore-size changes and responses of kaolinite with different structures subject to consolidation and shearing. *Engineering Geology*, 202, 122-131. http://dx.doi.org/10.1016/j.enggeo.2016.01.007.

Zhang, Y., Gallipoli, D., & Augarde, C. (2009). Simulation-based calibration of geotechnical parameters using parallel hybrid moving boundary particle swarm optimization. *Computers and Geotechnics*, 36(4), 604-615. http://dx.doi.org/10.1016/j.compgeo.2008.09.005.